Aerospace Science and Technology 84 (2019) 1150–1163

Contents lists available at ScienceDirect

Aerospace Science and Technology

www.elsevier.com/locate/aescte

Dynamic modelling and control of a Tendon-Actuated Lightweight Space Manipulator

Kai Li, Yao Zhang *, Quan Hu

School of Aerospace Engineering, Beijing Institute of Technology, 5 South Zhongguancun Street, Haidian District, Beijing 100081, China

ARTICLE INFO

Article history:
Received 3 April 2018
Received in revised form 21 October 2018
Accepted 11 November 2018
Available online 15 November 2018

Keywords:
Tendon-actuated manipulator
Dynamic modelling
Controller design
Tension analysis
Actuator model

ABSTRACT

The Tendon-Actuated Lightweight Space Manipulator has advantages such as a large range of motion and lightweight when compared with conventional space manipulators. In this paper, dynamic modelling and controller design of a tendon-actuated manipulator are investigated. First, nonlinear coupling dynamic equations of the central body spacecraft and a four-degree-of-freedom tendon-actuated manipulator mounted on it are derived based on Kane's equation, and their controllers are then designed while considering the dynamic coupling. In addition, a tension analysis method is proposed that is subject to the tension constraints, and the actuators of the tendon-actuated manipulator are analysed. Numerical simulations indicate that the designed controller can achieve attitude stability of the central body spacecraft and endpoint trajectory tracking of the tendon-actuated manipulator. A feature of the tendon-actuated manipulator is its enlargement of the joint actuated torque, and a long link, tendon-actuated manipulator has more benefits relative to a conventional space manipulator.

1. Introduction

Space manipulators play increasingly major roles in space activities such as spacecraft repair and assembly, on-orbit refuelling, capture of failed satellites and spacecraft inspections prior to re-entry because they can complete some dangerous and complex missions that are extremely difficult for astronauts.

The typical manipulator systems that have been used or demonstrated in practical space missions include the Shuttle Remote Manipulator System (SRMS), Space Station Remote Manipulator System (SSRMS), Japanese Experiment Module Remote Manipulator System (JEMRMS), European Robotic Arm (ERA) [1–3], ROTEX and ROKVISS [4]. All these conventional manipulator systems have similar structures that are comprised of carbon composite tubes and rotational joints, where two lightweight tubes are connected with a massive joint [5]. Therefore, if the tubes' lengths are increased, the actuated torques produced by the joints will increase simultaneously. Considering that a joint contains a motor, gear box, sensors and other components, the whole mass of the joint will increase greatly along with the increase in actuated torque. This will cause the total mass of the manipulator system to increase enormously, hugely increasing the expenses of aerospace activities finally. In view of this, a novel manipulator system named the Tendon-Actuated Lightweight Space Manipulator [6] has been designed and proposed that has features of dexterity, lightweight and versatility. In addition, the Tendon-Actuated Lightweight Space Manipulator has the following advantages: a large range of motion, high package efficiency and the ability to exert large tip forces [6]. Due to its merits when compared with conventional space manipulators, the novel Tendon-Actuated Lightweight Space Manipulator can be potentially applied in asteroid redirect missions and asteroid mining [7], i.e., capturing an entire free flying asteroid and retrieving a boulder on the surface of a large asteroid, respectively. In addition, some improvements to the Tendon-Actuated Lightweight Space Manipulator (let tendon-actuated manipulator represent the Tendon-Actuated Lightweight Space Manipulator in the following parts) are proposed such as multiple spreaders and telescoping links [8,9].

Some research regarding the tendon-actuated manipulator has been undertaken. Altenbuchner [10] utilised Finite Element software and MSC Adams to undertake a co-simulation using the flexible tendon-actuated manipulator to perform a satellite service mission. In addition, Altenbuchner [11] proposed proximity operation details for an asteroid redirect mission, and the co-simulation showed the dynamic response characteristics during the mission. Komendera et al. [5] derived the kinematics of the tendon-actuated manipulator and established the relation between joint angular velocity and motor velocity, a proportional-integral-derivative controller was then proposed, but only a proportional controller was

* Corresponding author.
E-mail addresses: likai_81@163.com (K. Li), zhangyao@bit.edu.cn (Y. Zhang), huquan2690@bit.edu.cn (Q. Hu).

https://doi.org/10.1016/j.ast.2018.11.018
1270-9638/

chosen for demonstration with tendon-actuated manipulator prototypes. In addition, they also analysed the tensions in the cables when utilising the tendon-actuated manipulator to manoeuvre and capture objects with different masses. However, the detailed dynamic equations of the tendon-actuated manipulator, considering the coupling characteristics between the tendon-actuated manipulator and the spacecraft bus, were not provided in all the current research mentioned above. The attitude motion of the base was also not considered. However, when the tendon-actuated manipulator is used in some space missions, it must be mounted on a spacecraft bus as the base platform to complete its work. Therefore, the interaction between the tendon-actuated manipulator and the spacecraft bus must be considered when establishing the dynamic equations of the system and analysing the dynamic characteristics. Therefore, the attitude controller of the spacecraft bus and the tracking controller of the tendon-actuated manipulator were not designed based on the above detailed dynamic equations in recent research. In addition, research on the method of designing the tensions in the cables also has not been performed. The reason why the link in the tendon-actuated manipulator can rotate is the equivalent joint actuated torque acted on the joint that is produced by the tensions in the cables. Thus, the method used to evaluate the tensions is important to control the tendon-actuated manipulator.

Much more research on the dynamics and control of conventional space manipulators has been undertaken, and many results have been obtained. This research can be used as a reference during dynamic modelling and controller design of the tendon-actuated manipulator. In dynamic modelling of a manipulator, the space manipulator system is considered to be a flexible multi-body system, and the general methods of establishing the dynamic equations of space manipulators include the Newton–Euler method [12–16], Lagrange method [17–20] and Kane method [21–23]. These three methods have their own features and can be used in different conditions. The Newton–Euler method needs to analyse every single body independently in the multibody system, and the constraint forces must be considered. The Lagrange method evaluates the energy of the multibody system by choosing the independent coordinates, but it involves a complex differentiation of a kinetic energy function. In addition, these two methods will confront difficulties as the degrees of freedom of the system are increased. Therefore, deriving dynamic equations based on the Kane method benefits from eliminating the constraint forces automatically and avoiding the complex operation of differentiating the energy function, especially for a system with multiple degrees of freedom. In addition, the dynamic equations obtained by the Kane method are suitable for numerical solution by computer [23]. Some other methods also have been developed to establish the dynamic equations of space manipulators, such as the Hamilton principle [24] and the Jourdain's velocity variation principle [25]. Xu et al. [26,27] analysed the dynamic coupling of space robots and proposed a method to identify the complete inertia parameters of space robotic system.

When undertaking a control design for a space manipulator, there are also some new methods. For example, Ulrich et al. [28–31] investigated the adaptive control of a flexible joint space manipulator under the condition of parametric uncertainties, but the base of the space manipulator was fixed. In Refs. [21,22] and [32,33], attitude control of the base and motion control of the space manipulator were considered simultaneously due to the dynamic coupling between the base and the space manipulator mounted on it. Virgili-Llop et al. [34] conducted laboratory experiments to demonstrate the autonomous capture of a space object by a space manipulator system, where controllers during different capture phases were designed. Zhang et al. [35] designed observer-based output feedback control strategy of space robotic manipulators based on fuzzy basis function network with the uncertainty of model considered. Huang et al. [36] designed a space debris removal system called dexterous tethered space robot and some ground experiments was done. In addition, a space manipulator that employs control moment gyroscopes as reactionless actuators was studied in Refs. [21] and [22]. Therefore, studying a space manipulator system while considering base motion and actuators contributes to an understanding of its dynamic characteristics.

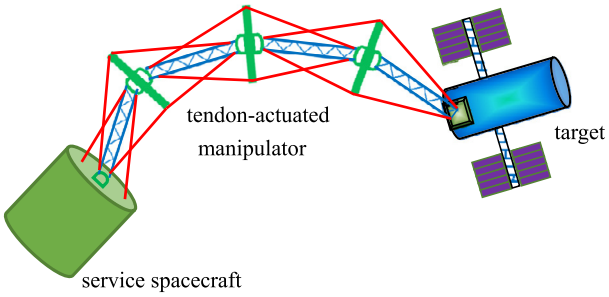

Fig. 1. A conceptual space mission of the tendon-actuated manipulator.

Therefore, in this paper, dynamic modelling and controller design of a four-degree-of-freedom tendon-actuated manipulator are investigated considering the above shortcomings. This manipulator is mounted on a free-flying central body spacecraft. Fig. 1 shows a conceptual space mission in which a service spacecraft employs the tendon-actuated manipulator to capture a target. First, the tendon-actuated manipulator system is simplified as a multi-rigid-body system under some assumptions. After the mass and the moment of inertia of the spreaders are equivalently converted into the corresponding links, the dynamic model of the tendon-actuated manipulator system in ordinary differential equation form is developed based on the Kane method. In addition, the relations between the tensions and the equivalent joint actuated torque are established. Second, the attitude controller of the central body spacecraft and trajectory tracking controller of the endpoint of the tendon-actuated manipulator are designed sequentially while considering dynamic coupling. A method of evaluating the tensions in the cables is then proposed that is subject to the tension constraints. In addition, characteristics of the actuators of the tendon-actuated manipulator are analysed in detail. At last, two simulation examples are provided based on different structural parameters of the tendon-actuated manipulator system.

2. Dynamic modelling of the tendon-actuated manipulator

The tendon-actuated manipulator system investigated in this paper consists of a central body spacecraft and a four-degree-of-freedom tendon-actuated manipulator mounted on it, as shown in Fig. 2. For the tendon-actuated manipulator, two adjacent links are connected with a revolute joint and the spreader rotates with the rotation of the corresponding joint. There are two cables (one is on the upper side of the two links and another is on the lower side) around one joint, where the left sides of them are both fixed on the left end of the left link, and the right sides are wound around the two capstans on the right end of the right link, respectively. The capstans are driven by the motors on the right end of every link so that the cables can be reeled in or out by the capstans. Then, the tendon-actuated manipulator can be driven by the equivalent joint actuated torque produced by the tensions in the cables. Compared with a conventional space manipulator, the actuated motors of the tendon-actuated manipulator are equipped on the right end of every link but not in the joint.

In this study, the central body spacecraft, the links and the spreaders are assumed as rigid body, respectively. Meanwhile, the deformation and the mass of the cables are neglected. The mass

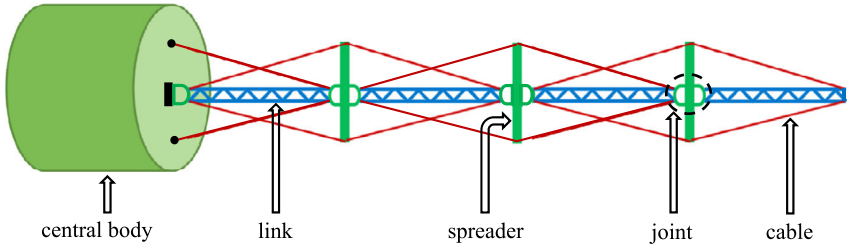

Fig. 2. Schematic of the tendon-actuated manipulator system.

and the moment of inertia of the spreaders are converted into the corresponding links. Then, the tendon-actuated manipulator system is viewed as a multi-rigid-body system.

2.1. Equivalent mass and inertia conversion of spreader

The kinematic relation between the spreader and the link is shown in Fig. 3, where $O_i x_i y_i z_i$ $(i = 1, 2, 3, 4)$ and $O_i x_s y_s z_s$ are the body fixed frame of the link i and the corresponding spreader, respectively. The y_i-axis and the y_s-axis coincide with the rotation direction of the joint i and are perpendicular to the $x_i z_i$ plane, which are not shown in Fig. 3. θ_i is the ith joint angle. When the link i rotates relative to the link $i-1$ around the y_i-axis, the spreader rotates around the y_i-axis simultaneously, and the z_s-axis always bisects the angle between the link i and the link $i-1$. Then, the mass and the moment of inertia of the spreader can be equivalently converted into the link i because the rotation of the spreader can only affect the rotation of the link i. Therefore, the equivalent mass of the link i is

$$m_{ei} = m_i + m_s \tag{1}$$

where m_i, m_s and m_{ei} represent the mass of the link i, the mass of the spreader and the equivalent mass of the link i, respectively.

The equivalent moment of inertia of the link i is

$$\boldsymbol{I}_{ei} = \boldsymbol{I}_i + \boldsymbol{L}_y\left(\frac{\theta_i}{2}\right)\boldsymbol{I}_s \tag{2}$$

where $\boldsymbol{I}_i$, $\boldsymbol{I}_s$ and $\boldsymbol{I}_{ei}$ represent the moment of inertia of the link i, the moment of inertia of the spreader and the equivalent moment of inertia of the link i, respectively. $\boldsymbol{L}_y(\lambda)$ is the unit rotation matrix that represents a rotation around the y-axis by angle λ and is given by

$$\boldsymbol{L}_y(\lambda) = \begin{bmatrix} \cos\lambda & 0 & -\sin\lambda \\ 0 & 1 & 0 \\ \sin\lambda & 0 & \cos\lambda \end{bmatrix} \tag{3}$$

If the spreader and the link i are both rotating in the $x_i y_i$ plane around the z_i-axis, then the moment of inertia of the spreader can be converted similarly and $\boldsymbol{L}_z(\lambda)$ can be analogously defined:

$$\boldsymbol{L}_z(\lambda) = \begin{bmatrix} \cos\lambda & \sin\lambda & 0 \\ -\sin\lambda & \cos\lambda & 0 \\ 0 & 0 & 1 \end{bmatrix} \tag{4}$$

2.2. Dynamic equations

According to the assumptions mentioned above, the tendon-actuated manipulator system can be simplified as a multi-rigid-body system shown in Fig. 4, which is composed of a free-floating central body spacecraft and a four-degree-of-freedom manipulator. To obtain a general form of the dynamic equations, every joint

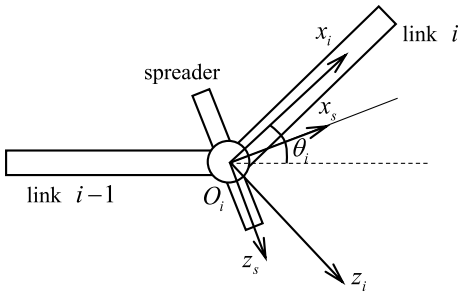

Fig. 3. Rotation of the spreader and the link.

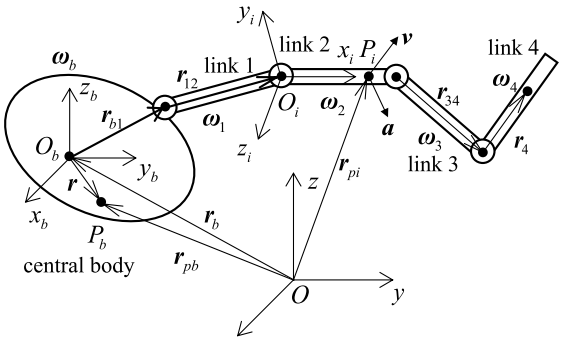

Fig. 4. Simplified tendon-actuated manipulator system.

is assumed to have three rotational degrees of freedom. And the real dynamic equations of the tendon-actuated manipulator system whose joint has one rotational degree of freedom in this study can be easily derived from the general form using the kinematic relations discussed in following.

Some symbols and variables in Fig. 4 are defined as follows. $Oxyz$ and $O_b x_b y_b z_b$ are the inertial frame and the body fixed frame of the central body spacecraft, respectively. O_b is the centroid of the central body spacecraft. $\boldsymbol{r}_b$ is the position vector of O_b. $\boldsymbol{r}_{b1}$ is the position vector from O_b to the joint 1. $\boldsymbol{r}_{j(j+1)}$ $(j = 1, 2, 3)$ is the position vector from the jth joint to the $(j+1)$th joint. $\boldsymbol{\omega}_b$ is the angular velocity of the central body spacecraft. $\boldsymbol{\omega}_i$ $(i = 1, 2, 3, 4)$ is the angular velocity of the link i relative to its inner body.

The generalised speeds written in column matrix form are adopted to describe the motion of the simplified tendon-actuated manipulator system, and they are defined as

$$\begin{aligned} &\boldsymbol{u}_1 = \dot{\boldsymbol{r}}_b, \quad \boldsymbol{u}_2 = \boldsymbol{\omega}_b, \quad \boldsymbol{u}_3 = \boldsymbol{\omega}_1, \quad \boldsymbol{u}_4 = \boldsymbol{\omega}_2, \\ &\boldsymbol{u}_5 = \boldsymbol{\omega}_3, \quad \boldsymbol{u}_6 = \boldsymbol{\omega}_4 \end{aligned} \tag{5}$$

where $\dot{\boldsymbol{r}}_b$ represents the velocity of the centroid of the central body spacecraft.

Meanwhile, the corresponding generalised coordinates are also defined as

$$\boldsymbol{q}_1=\boldsymbol{r}_b,\quad \boldsymbol{q}_2=\boldsymbol{\Theta}_b,\quad \boldsymbol{q}_3=\boldsymbol{\Theta}_1,\quad \boldsymbol{q}_4=\boldsymbol{\Theta}_2,$$
$$\boldsymbol{q}_5=\boldsymbol{\Theta}_3,\quad \boldsymbol{q}_6=\boldsymbol{\Theta}_4 \tag{6}$$

where the generalised speeds are differentials of the generalised coordinates, that is $\dot{\boldsymbol{q}}_r=\boldsymbol{u}_r$ $(r=1,2,...,6)$.

Therefore, the inertial velocity for a generic point in the simplified tendon-actuated manipulator system can be written as a combination of the generalised speeds:

$$\boldsymbol{v}_g=\sum_{r=1}^{6}\boldsymbol{G}_{gr}\boldsymbol{u}_r \tag{7}$$

where $\boldsymbol{G}_{gr}$ represents the partial velocity matrix of an arbitrary point in body g corresponding to the rth generalised speed $\boldsymbol{u}_r$, and body g represents the central body spacecraft or the link i in the simplified tendon-actuated manipulator system. Differentiating Eq. (7), the acceleration for a generic point can be obtained:

$$\boldsymbol{a}_g=\sum_{r=1}^{6}\boldsymbol{G}_{gr}\dot{\boldsymbol{u}}_r+\sum_{r=1}^{6}\dot{\boldsymbol{G}}_{gr}\boldsymbol{u}_r \tag{8}$$

The general matrix form of Kane's equations can be written as

$$\boldsymbol{f}_{Ik}+\boldsymbol{f}_{ek}=0,\quad k=1,2,...,n \tag{9}$$

where $\boldsymbol{f}_{Ik}$ and $\boldsymbol{f}_{ek}$ are the kth generalised inertia force and the kth generalised external force corresponding to the kth generalised speed, respectively. In addition, n is the number of generalised speeds written in column matrix form. For the simplified tendon-actuated manipulator system shown in Fig. 4, $n=6$.

The kth generalised inertia force for the simplified system shown in Fig. 4 is evaluated by

$$\boldsymbol{f}_{Ik}=-\int_B \boldsymbol{G}_{gr}^T\boldsymbol{a}_g dm \tag{10}$$

For the simplified system shown in Fig. 4, $\boldsymbol{F}$ represents the concentrated force acted on the centroid of the central body spacecraft. $\boldsymbol{T}$ and $\boldsymbol{T}_i$ are the control torques acted on the central body spacecraft and joint i, respectively. For convenience, the external force and torque are rewritten as

$$\boldsymbol{F}_{a1}=\boldsymbol{F},\quad \boldsymbol{F}_{a2}=\boldsymbol{T},\quad \boldsymbol{F}_{a3}=\boldsymbol{T}_1,\quad \boldsymbol{F}_{a4}=\boldsymbol{T}_2,$$
$$\boldsymbol{F}_{a5}=\boldsymbol{T}_3,\quad \boldsymbol{F}_{a6}=\boldsymbol{T}_4 \tag{11}$$

The virtual work of the simplified system is calculated by

$$\delta W=\sum_{r=1}^{6}\boldsymbol{F}_{ar}^T\delta\boldsymbol{q}_r \tag{12}$$

Consequently, the kth generalised external force is given by

$$\boldsymbol{f}_{ek}=\boldsymbol{F}_{ak} \tag{13}$$

Substituting Eqs. (10) and (13) into Eq. (9), a general form of the dynamic equations of the simplified tendon-actuated manipulator system is obtained:

$$\boldsymbol{M}\dot{\boldsymbol{u}}+\boldsymbol{F}_c=\boldsymbol{\tau} \tag{14}$$

where $\boldsymbol{M}$ is the 18×18 symmetric mass matrix of the tendon-actuated manipulator system; $\boldsymbol{u}=\left[\begin{array}{cccc}\boldsymbol{u}_1^T & \boldsymbol{u}_2^T & \cdots & \boldsymbol{u}_6^T\end{array}\right]^T$ is the generalised speed column matrix; $\boldsymbol{F}_c$ is the nonlinear coupled term; and $\boldsymbol{\tau}=\left[\begin{array}{cccc}\boldsymbol{F}_{a1}^T & \boldsymbol{F}_{a2}^T & \cdots & \boldsymbol{F}_{a6}^T\end{array}\right]^T$ is the generalised external force column matrix. The detail expression for $\boldsymbol{M}$ is given by

$$\boldsymbol{M}=\begin{bmatrix}
m\boldsymbol{I}_{3\times3} & -\boldsymbol{A}_{Ib}\tilde{\boldsymbol{S}}_t & -\boldsymbol{A}_{I1}\tilde{\boldsymbol{S}}_{1t} & -\boldsymbol{A}_{I2}\tilde{\boldsymbol{S}}_{2t} & -\boldsymbol{A}_{I3}\tilde{\boldsymbol{S}}_{3t} & -\boldsymbol{A}_{I4}\tilde{\boldsymbol{S}}_{4t}\\
-\tilde{\boldsymbol{S}}_t^T\boldsymbol{A}_{bI} & \boldsymbol{I}_t & \boldsymbol{A}_{b1}\boldsymbol{I}_{1_o} & \boldsymbol{A}_{b2}\boldsymbol{I}_{2_o} & \boldsymbol{A}_{b3}\boldsymbol{I}_{3_o} & \boldsymbol{A}_{b4}\boldsymbol{I}_{4_o}\\
-\tilde{\boldsymbol{S}}_{1t}^T\boldsymbol{A}_{1I} & \boldsymbol{I}_{1_o}^T\boldsymbol{A}_{1b} & \boldsymbol{I}_{1t} & \boldsymbol{A}_{12}\boldsymbol{I}_{2_1} & \boldsymbol{A}_{13}\boldsymbol{I}_{3_1} & \boldsymbol{A}_{14}\boldsymbol{I}_{4_1}\\
-\tilde{\boldsymbol{S}}_{2t}^T\boldsymbol{A}_{2I} & \boldsymbol{I}_{2_o}^T\boldsymbol{A}_{2b} & \boldsymbol{I}_{2_1}^T\boldsymbol{A}_{21} & \boldsymbol{I}_{2t} & \boldsymbol{A}_{23}\boldsymbol{I}_{3_2} & \boldsymbol{A}_{24}\boldsymbol{I}_{4_2}\\
-\tilde{\boldsymbol{S}}_{3t}^T\boldsymbol{A}_{3I} & \boldsymbol{I}_{3_o}^T\boldsymbol{A}_{3b} & \boldsymbol{I}_{3_1}^T\boldsymbol{A}_{31} & \boldsymbol{I}_{3_2}^T\boldsymbol{A}_{32} & \boldsymbol{I}_{3t} & \boldsymbol{A}_{34}\boldsymbol{I}_{4_3}\\
-\tilde{\boldsymbol{S}}_{4t}^T\boldsymbol{A}_{4I} & \boldsymbol{I}_{4_o}^T\boldsymbol{A}_{4b} & \boldsymbol{I}_{4_1}^T\boldsymbol{A}_{41} & \boldsymbol{I}_{4_2}^T\boldsymbol{A}_{42} & \boldsymbol{I}_{4_3}^T\boldsymbol{A}_{43} & \boldsymbol{I}_{4t}
\end{bmatrix} \tag{15}$$

The nonlinear coupled term is

$$\boldsymbol{F}_c=\left[\begin{array}{cccccc}\boldsymbol{F}_{cr}^T & \boldsymbol{F}_{c\omega}^T & \boldsymbol{F}_{c\omega_1}^T & \boldsymbol{F}_{c\omega_2}^T & \boldsymbol{F}_{c\omega_3}^T & \boldsymbol{F}_{c\omega_4}^T\end{array}\right]^T \tag{16}$$

where

$$\begin{aligned}\boldsymbol{F}_{cr}=&-\boldsymbol{A}_{Ib}\tilde{\boldsymbol{\omega}}_b\tilde{\boldsymbol{S}}_b^*\boldsymbol{\omega}_b-\left(\boldsymbol{A}_{I1}\tilde{\boldsymbol{\Omega}}_1\tilde{\boldsymbol{S}}_1^*\boldsymbol{\Omega}_1+\boldsymbol{A}_{I2}\tilde{\boldsymbol{\Omega}}_2\tilde{\boldsymbol{S}}_2^*\boldsymbol{\Omega}_2\right.\\&\left.+\boldsymbol{A}_{I3}\tilde{\boldsymbol{\Omega}}_3\tilde{\boldsymbol{S}}_3^*\boldsymbol{\Omega}_3+\boldsymbol{A}_{I4}\tilde{\boldsymbol{\Omega}}_4\tilde{\boldsymbol{S}}_4^*\boldsymbol{\Omega}_4\right)-\left(\boldsymbol{A}_{I1}\tilde{\boldsymbol{S}}_{1t}\boldsymbol{A}_{1b}\tilde{\boldsymbol{\omega}}_b\boldsymbol{A}_{b1}\boldsymbol{\Omega}_1\right.\\&+\boldsymbol{A}_{I2}\tilde{\boldsymbol{S}}_{2t}\boldsymbol{A}_{21}\tilde{\boldsymbol{\Omega}}_1\boldsymbol{A}_{12}\boldsymbol{\Omega}_2+\boldsymbol{A}_{I3}\tilde{\boldsymbol{S}}_{3t}\boldsymbol{A}_{32}\tilde{\boldsymbol{\Omega}}_2\boldsymbol{A}_{23}\boldsymbol{\Omega}_3\\&\left.+\boldsymbol{A}_{I4}\tilde{\boldsymbol{S}}_{4t}\boldsymbol{A}_{43}\tilde{\boldsymbol{\Omega}}_3\boldsymbol{A}_{34}\boldsymbol{\Omega}_4\right)\end{aligned} \tag{17}$$

$$\begin{aligned}\boldsymbol{F}_{c\omega}=&\boldsymbol{I}_\omega\boldsymbol{\omega}_b+\boldsymbol{A}_{b1}\boldsymbol{I}_{\Omega_{1\_o}}\boldsymbol{\Omega}_1+\boldsymbol{A}_{b2}\boldsymbol{I}_{\Omega_{2\_o}}\boldsymbol{\Omega}_2+\boldsymbol{A}_{b3}\boldsymbol{I}_{\Omega_{3\_o}}\boldsymbol{\Omega}_3\\&+\boldsymbol{A}_{b4}\boldsymbol{I}_{\Omega_{4\_o}}\boldsymbol{\Omega}_4+\boldsymbol{A}_{b1}\boldsymbol{I}_{1\_o}\boldsymbol{A}_{1b}\tilde{\boldsymbol{\omega}}_b\boldsymbol{A}_{b1}\boldsymbol{\Omega}_1\\&+\boldsymbol{A}_{b2}\boldsymbol{I}_{2\_o}\boldsymbol{A}_{21}\tilde{\boldsymbol{\Omega}}_1\boldsymbol{A}_{12}\boldsymbol{\Omega}_2+\boldsymbol{A}_{b3}\boldsymbol{I}_{3\_o}\boldsymbol{A}_{32}\tilde{\boldsymbol{\Omega}}_2\boldsymbol{A}_{23}\boldsymbol{\Omega}_3\\&+\boldsymbol{A}_{b4}\boldsymbol{I}_{4\_o}\boldsymbol{A}_{43}\tilde{\boldsymbol{\Omega}}_3\boldsymbol{A}_{34}\boldsymbol{\Omega}_4\end{aligned} \tag{18}$$

$$\begin{aligned}\boldsymbol{F}_{c\omega_1}=&\tilde{\boldsymbol{S}}_{1t}^T\boldsymbol{A}_{1b}\tilde{\boldsymbol{\omega}}_b\tilde{\boldsymbol{r}}_{b1}\boldsymbol{\omega}_b+\boldsymbol{I}_{\Omega_1}\boldsymbol{\Omega}_1+\boldsymbol{A}_{12}\boldsymbol{I}_{\Omega_{2\_1}}\boldsymbol{\Omega}_2\\&+\boldsymbol{A}_{13}\boldsymbol{I}_{\Omega_{3\_1}}\boldsymbol{\Omega}_3+\boldsymbol{A}_{14}\boldsymbol{I}_{\Omega_{4\_1}}\boldsymbol{\Omega}_4+\boldsymbol{I}_{1t}\boldsymbol{A}_{1b}\tilde{\boldsymbol{\omega}}_b\boldsymbol{A}_{b1}\boldsymbol{\Omega}_1\\&+\boldsymbol{A}_{12}\boldsymbol{I}_{2\_1}\boldsymbol{A}_{21}\tilde{\boldsymbol{\Omega}}_1\boldsymbol{A}_{12}\boldsymbol{\Omega}_2+\boldsymbol{A}_{13}\boldsymbol{I}_{3\_1}\boldsymbol{A}_{32}\tilde{\boldsymbol{\Omega}}_2\boldsymbol{A}_{23}\boldsymbol{\Omega}_3\\&+\boldsymbol{A}_{14}\boldsymbol{I}_{4\_1}\boldsymbol{A}_{43}\tilde{\boldsymbol{\Omega}}_3\boldsymbol{A}_{34}\boldsymbol{\Omega}_4\end{aligned} \tag{19}$$

$$\begin{aligned}\boldsymbol{F}_{c\omega_2}=&\tilde{\boldsymbol{S}}_{2t}^T\boldsymbol{A}_{2b}\tilde{\boldsymbol{\omega}}_b\tilde{\boldsymbol{r}}_{b1}\boldsymbol{\omega}_b+\boldsymbol{A}_{21}\boldsymbol{I}_{\Omega_{1\_2}}\boldsymbol{\Omega}_1+\boldsymbol{I}_{\Omega_2}\boldsymbol{\Omega}_2\\&+\boldsymbol{A}_{23}\boldsymbol{I}_{\Omega_{3\_2}}\boldsymbol{\Omega}_3+\boldsymbol{A}_{24}\boldsymbol{I}_{\Omega_{4\_2}}\boldsymbol{\Omega}_4+\boldsymbol{I}_{2\_1}^T\boldsymbol{A}_{2b}\tilde{\boldsymbol{\omega}}_b\boldsymbol{A}_{b1}\boldsymbol{\Omega}_1\\&+\boldsymbol{I}_{2t}\boldsymbol{A}_{21}\tilde{\boldsymbol{\Omega}}_1\boldsymbol{A}_{12}\boldsymbol{\Omega}_2+\boldsymbol{A}_{23}\boldsymbol{I}_{3\_2}\boldsymbol{A}_{32}\tilde{\boldsymbol{\Omega}}_2\boldsymbol{A}_{23}\boldsymbol{\Omega}_3\\&+\boldsymbol{A}_{24}\boldsymbol{I}_{4\_2}\boldsymbol{A}_{43}\tilde{\boldsymbol{\Omega}}_3\boldsymbol{A}_{34}\boldsymbol{\Omega}_4\end{aligned} \tag{20}$$

$$\begin{aligned}\boldsymbol{F}_{c\omega_3}=&\tilde{\boldsymbol{S}}_{3t}^T\boldsymbol{A}_{3b}\tilde{\boldsymbol{\omega}}_b\tilde{\boldsymbol{r}}_{b1}\boldsymbol{\omega}_b+\boldsymbol{A}_{31}\boldsymbol{I}_{\Omega_{1\_3}}\boldsymbol{\Omega}_1+\boldsymbol{A}_{32}\boldsymbol{I}_{\Omega_{2\_3}}\boldsymbol{\Omega}_2\\&+\boldsymbol{I}_{\Omega_3}\boldsymbol{\Omega}_3+\boldsymbol{A}_{34}\boldsymbol{I}_{\Omega_{4\_3}}\boldsymbol{\Omega}_4+\boldsymbol{I}_{3\_1}^T\boldsymbol{A}_{3b}\tilde{\boldsymbol{\omega}}_b\boldsymbol{A}_{b1}\boldsymbol{\Omega}_1\\&+\boldsymbol{I}_{3\_2}^T\boldsymbol{A}_{31}\tilde{\boldsymbol{\Omega}}_1\boldsymbol{A}_{12}\boldsymbol{\Omega}_2+\boldsymbol{I}_{3t}\boldsymbol{A}_{32}\tilde{\boldsymbol{\Omega}}_2\boldsymbol{A}_{23}\boldsymbol{\Omega}_3\\&+\boldsymbol{A}_{34}\boldsymbol{I}_{4\_3}\boldsymbol{A}_{43}\tilde{\boldsymbol{\Omega}}_3\boldsymbol{A}_{34}\boldsymbol{\Omega}_4\end{aligned} \tag{21}$$

$$\begin{aligned}\boldsymbol{F}_{c\omega_4}=&\tilde{\boldsymbol{S}}_{4t}^T\boldsymbol{A}_{4b}\tilde{\boldsymbol{\omega}}_b\tilde{\boldsymbol{r}}_{b1}\boldsymbol{\omega}_b+\boldsymbol{A}_{41}\boldsymbol{I}_{\Omega_{1\_4}}\boldsymbol{\Omega}_1+\boldsymbol{A}_{42}\boldsymbol{I}_{\Omega_{2\_4}}\boldsymbol{\Omega}_2\\&+\boldsymbol{A}_{43}\boldsymbol{I}_{\Omega_{3\_4}}\boldsymbol{\Omega}_3+\boldsymbol{I}_{\Omega_4}\boldsymbol{\Omega}_4+\boldsymbol{I}_{4\_1}^T\boldsymbol{A}_{4b}\tilde{\boldsymbol{\omega}}_b\boldsymbol{A}_{b1}\boldsymbol{\Omega}_1\\&+\boldsymbol{I}_{4\_2}^T\boldsymbol{A}_{41}\tilde{\boldsymbol{\Omega}}_1\boldsymbol{A}_{12}\boldsymbol{\Omega}_2+\boldsymbol{I}_{4\_3}^T\boldsymbol{A}_{42}\tilde{\boldsymbol{\Omega}}_2\boldsymbol{A}_{23}\boldsymbol{\Omega}_3\\&+\boldsymbol{I}_{4t}\boldsymbol{A}_{43}\tilde{\boldsymbol{\Omega}}_3\boldsymbol{A}_{34}\boldsymbol{\Omega}_4\end{aligned} \tag{22}$$

The general nonlinear dynamic equations of the simplified multi-rigid-body system shown in Fig. 4 can be described by Eq. (14). This equation allows the joint to have three rotational degrees of freedom. However, the joint of the tendon-actuated manipulator usually has only one rotational degree of freedom. Therefore, Eq. (14) can be written in a new form considering the kinematics of the central body spacecraft and the joint.

For the central body spacecraft, the z–x–y Euler angle sequence is adopted to describe its attitude. Let $\boldsymbol{\Phi}_b=\left[\begin{array}{ccc}\varphi & \theta & \psi\end{array}\right]^T$, where φ, θ and ψ are roll angle, pitch angle and yaw angle, respectively. The attitude kinematical equation of the central body spacecraft is then given by

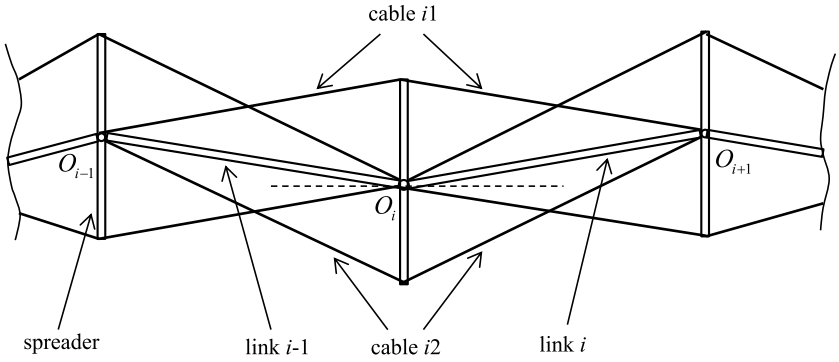

Fig. 5. Partial structure of the tendon-actuated manipulator.

$$\boldsymbol{\omega}_b = \boldsymbol{H}_b \dot{\boldsymbol{\Phi}}_b \tag{23}$$

where $\boldsymbol{H}_b$ is a 3×3 matrix determined by the Euler angles, the expression of which is given by

$$\boldsymbol{H}_b = \begin{bmatrix} \cos\theta & 0 & -\cos\varphi\sin\theta \\ 0 & 1 & \sin\varphi \\ \sin\theta & 0 & \cos\varphi\cos\theta \end{bmatrix} \tag{24}$$

Differentiating Eq. (23) returns

$$\dot{\boldsymbol{\omega}}_b = \boldsymbol{H}_b \ddot{\boldsymbol{\Phi}}_b + \boldsymbol{H}_{bc} \dot{\boldsymbol{\Phi}}_{bc} \tag{25}$$

where $\dot{\boldsymbol{\Phi}}_{bc} = \begin{bmatrix} \dot{\varphi}\dot{\theta} & \dot{\theta}\dot{\psi} & \dot{\psi}\dot{\varphi} \end{bmatrix}^T$, and $\boldsymbol{H}_{bc}$ is a 3×3 matrix given by

$$\boldsymbol{H}_{bc} = \begin{bmatrix} -\sin\theta & -\cos\varphi\cos\theta & \sin\varphi\sin\theta \\ 0 & 0 & \cos\varphi \\ \cos\theta & -\cos\varphi\sin\theta & -\sin\varphi\cos\theta \end{bmatrix} \tag{26}$$

The joint in the tendon-actuated manipulator investigated in this study shown in Fig. 2 is regarded as a revolute joint so that the relative rotational angle θ_i is defined to describe the relative rotation of the link i. That is to say, every link in the tendon-actuated manipulator has only one rotational degree of freedom. Therefore, the kinematical equation of the link i relative to the link $i-1$ is expressed as

$$\boldsymbol{\omega}_i = \boldsymbol{\eta}_i \dot{\theta}_i \tag{27}$$

where $\boldsymbol{\eta}_i$ is a 3×1 column matrix described the relative rotation direction of the link i and expressed in the body fixed frame $O_i x_i y_i z_i$. Substituting Eq. (27) into Eq. (14), the dynamic equations of the tendon-actuated manipulator system are rearranged as

$$\boldsymbol{M}_e \dot{\boldsymbol{u}}_e + \boldsymbol{F}_c^e = \boldsymbol{\tau}_e \tag{28}$$

where $\boldsymbol{M}_e$ is the 10×10 new symmetric mass matrix of the tendon-actuated manipulator system; $\boldsymbol{u}_e = \begin{bmatrix} \dot{\boldsymbol{r}}_b^T & \boldsymbol{\omega}_b^T & \dot{\theta}_1 & \dot{\theta}_2 & \dot{\theta}_3 & \dot{\theta}_4 \end{bmatrix}^T$ is the new generalised speed column matrix; $\boldsymbol{F}_c^e$ is the new nonlinear coupled term; and $\boldsymbol{\tau}_e = \begin{bmatrix} \boldsymbol{F}^T & \boldsymbol{T}^T & T_1 & T_2 & T_3 & T_4 \end{bmatrix}^T$ is the new generalised external force column matrix, where $T_i = \boldsymbol{\eta}_i^T \boldsymbol{T}_i$ represents the actuated torque acted on the ith revolute joint. The expressions for $\boldsymbol{M}_e$ and $\boldsymbol{F}_c^e$ are

$$\boldsymbol{M}_e = \begin{bmatrix} m\boldsymbol{I}_{3\times3} & -\boldsymbol{A}_{1b}\tilde{\boldsymbol{S}}_t & -\boldsymbol{A}_{l1}\tilde{\boldsymbol{S}}_{1t}\boldsymbol{\eta}_1 & -\boldsymbol{A}_{l2}\tilde{\boldsymbol{S}}_{2t}\boldsymbol{\eta}_2 & -\boldsymbol{A}_{l3}\tilde{\boldsymbol{S}}_{3t}\boldsymbol{\eta}_3 & -\boldsymbol{A}_{l4}\tilde{\boldsymbol{S}}_{4t}\boldsymbol{\eta}_4 \\ -\tilde{\boldsymbol{S}}_t^T\boldsymbol{A}_{bl} & \boldsymbol{I}_t & \boldsymbol{A}_{b1}\boldsymbol{I}_{1\_o}\boldsymbol{\eta}_1 & \boldsymbol{A}_{b2}\boldsymbol{I}_{2\_o}\boldsymbol{\eta}_2 & \boldsymbol{A}_{b3}\boldsymbol{I}_{3\_o}\boldsymbol{\eta}_3 & \boldsymbol{A}_{b4}\boldsymbol{I}_{4\_o}\boldsymbol{\eta}_4 \\ -\boldsymbol{\eta}_1^T\tilde{\boldsymbol{S}}_{1t}^T\boldsymbol{A}_{1l} & \boldsymbol{\eta}_1^T\boldsymbol{I}_{1\_o}^T\boldsymbol{A}_{1b} & \boldsymbol{\eta}_1^T\boldsymbol{I}_{1t}\boldsymbol{\eta}_1 & \boldsymbol{\eta}_1^T\boldsymbol{A}_{12}\boldsymbol{I}_{2\_1}\boldsymbol{\eta}_2 & \boldsymbol{\eta}_1^T\boldsymbol{A}_{13}\boldsymbol{I}_{3\_1}\boldsymbol{\eta}_3 & \boldsymbol{\eta}_1^T\boldsymbol{A}_{14}\boldsymbol{I}_{4\_1}\boldsymbol{\eta}_4 \\ -\boldsymbol{\eta}_2^T\tilde{\boldsymbol{S}}_{2t}^T\boldsymbol{A}_{2l} & \boldsymbol{\eta}_2^T\boldsymbol{I}_{2\_o}^T\boldsymbol{A}_{2b} & \boldsymbol{\eta}_2^T\boldsymbol{I}_{2\_1}^T\boldsymbol{A}_{21}\boldsymbol{\eta}_1 & \boldsymbol{\eta}_2^T\boldsymbol{I}_{2t}\boldsymbol{\eta}_2 & \boldsymbol{\eta}_2^T\boldsymbol{A}_{23}\boldsymbol{I}_{3\_2}\boldsymbol{\eta}_3 & \boldsymbol{\eta}_2^T\boldsymbol{A}_{24}\boldsymbol{I}_{4\_2}\boldsymbol{\eta}_4 \\ -\boldsymbol{\eta}_3^T\tilde{\boldsymbol{S}}_{3t}^T\boldsymbol{A}_{3l} & \boldsymbol{\eta}_3^T\boldsymbol{I}_{3\_o}^T\boldsymbol{A}_{3b} & \boldsymbol{\eta}_3^T\boldsymbol{I}_{3\_1}^T\boldsymbol{A}_{31}\boldsymbol{\eta}_1 & \boldsymbol{\eta}_3^T\boldsymbol{I}_{3\_2}^T\boldsymbol{A}_{32}\boldsymbol{\eta}_2 & \boldsymbol{\eta}_3^T\boldsymbol{I}_{3t}\boldsymbol{\eta}_3 & \boldsymbol{\eta}_3^T\boldsymbol{A}_{34}\boldsymbol{I}_{4\_3}\boldsymbol{\eta}_4 \\ -\boldsymbol{\eta}_4^T\tilde{\boldsymbol{S}}_{4t}^T\boldsymbol{A}_{4l} & \boldsymbol{\eta}_4^T\boldsymbol{I}_{4\_o}^T\boldsymbol{A}_{4b} & \boldsymbol{\eta}_4^T\boldsymbol{I}_{4\_1}^T\boldsymbol{A}_{41}\boldsymbol{\eta}_1 & \boldsymbol{\eta}_4^T\boldsymbol{I}_{4\_2}^T\boldsymbol{A}_{42}\boldsymbol{\eta}_2 & \boldsymbol{\eta}_4^T\boldsymbol{I}_{4\_3}^T\boldsymbol{A}_{43}\boldsymbol{\eta}_3 & \boldsymbol{\eta}_4^T\boldsymbol{I}_{4t}\boldsymbol{\eta}_4 \end{bmatrix} \tag{29}$$

$$\boldsymbol{F}_c^e = \begin{bmatrix} (\boldsymbol{F}_{cr}^e)^T & (\boldsymbol{F}_{c\omega}^e)^T & (\boldsymbol{F}_{cm}^e)^T \end{bmatrix}^T \tag{30}$$

where

$$\boldsymbol{F}_{cr}^e = \boldsymbol{F}_{cr}, \qquad \boldsymbol{F}_{c\omega}^e = \boldsymbol{F}_{c\omega} \tag{31}$$

$$\boldsymbol{F}_{cm}^e = \begin{bmatrix} \boldsymbol{\eta}_1^T\boldsymbol{F}_{c\omega_1} & \boldsymbol{\eta}_2^T\boldsymbol{F}_{c\omega_2} & \boldsymbol{\eta}_3^T\boldsymbol{F}_{c\omega_3} & \boldsymbol{\eta}_4^T\boldsymbol{F}_{c\omega_4} \end{bmatrix}^T \tag{32}$$

The actuated motors of the tendon-actuated manipulator are equipped on the right end of every link, and the joint actuated torque is therefore equivalently produced by the tensions in the cables, as shown in Fig. 5. There are two cables around one joint (cable $i1$ and cable $i2$ for joint i), and the equivalent joint actuated torque is only determined by the tensions in the two cables. The link i is chosen as an example to analyse the relations between the tensions and the equivalent joint actuated torque, which is shown in Fig. 6. N_i^{c1} and N_i^{c2} are the tensions in the cable $i1$ and cable $i2$, respectively. When evaluating the equivalent joint actuated torque of the ith joint, the tensions N_i^{c1} and N_i^{c2} are only considered because the torque produced by the tensions N_{i+1}^{c1} and N_{i+1}^{c2} is equal to zero. The equivalent joint actuated torque of the ith joint is given by

$$M_i = N_i^{c1} l_{i1} - N_i^{c2} l_{i2} \tag{33}$$

where l_{i1} and l_{i2} are obtained by the geometrical relations shown in Fig. 6:

$$\begin{aligned} l_{i1} &= \frac{Ld\cos\frac{\theta_i}{2}}{2\sqrt{L^2 + \frac{d^2}{4} - Ld\sin\frac{\theta_i}{2}}}, \\ l_{i2} &= \frac{Ld\cos\frac{\theta_i}{2}}{2\sqrt{L^2 + \frac{d^2}{4} + Ld\sin\frac{\theta_i}{2}}} \end{aligned} \tag{34}$$

where L and d are the length of the link and the spreader, respectively.

Considering the four links in the tendon-actuated manipulator system shown in Fig. 2 and combining Eq. (33), the relation between the equivalent joint actuated torque of the four joints and the tensions in all the cables can be written in the matrix form

$$\boldsymbol{T}_m = \boldsymbol{D}\boldsymbol{x}, \tag{35}$$

where $\boldsymbol{D}$ is a 4×8 matrix determined by the joint angles; $\boldsymbol{x} = \begin{bmatrix} N_1^{c1} & N_1^{c2} & N_2^{c1} & N_2^{c2} & N_3^{c1} & N_3^{c2} & N_4^{c1} & N_4^{c2} \end{bmatrix}^T$ represents the tension column matrix; $\boldsymbol{T}_m = \begin{bmatrix} T_1 & T_2 & T_3 & T_4 \end{bmatrix}^T$ represents the equivalent joint actuated torque column matrix.

The motion of the tendon-actuated manipulator system can be divided into the translation and rotation of the central body spacecraft and the motion of the manipulator. Hence, Eq. (28) can be rearranged as

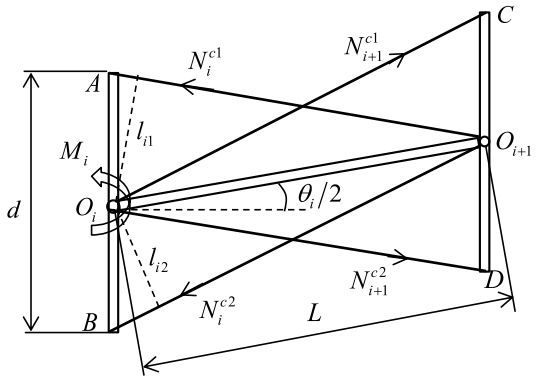

Fig. 6. Schematic of the equivalent joint actuated torque and the tensions.

$$\begin{bmatrix} \boldsymbol{M}_r & \boldsymbol{M}_{r\omega} & \boldsymbol{M}_{rm} \\ \boldsymbol{M}_{\omega r} & \boldsymbol{M}_{\omega} & \boldsymbol{M}_{\omega m} \\ \boldsymbol{M}_{mr} & \boldsymbol{M}_{m\omega} & \boldsymbol{M}_m \end{bmatrix} \begin{bmatrix} \ddot{\boldsymbol{r}}_b \\ \dot{\boldsymbol{\omega}}_b \\ \ddot{\boldsymbol{\theta}}_m \end{bmatrix} + \begin{bmatrix} \boldsymbol{F}_{cr}^e \\ \boldsymbol{F}_{c\omega}^e \\ \boldsymbol{F}_{cm}^e \end{bmatrix} = \begin{bmatrix} \boldsymbol{F} \\ \boldsymbol{T} \\ \boldsymbol{T}_m \end{bmatrix} \tag{36}$$

where $\boldsymbol{\theta}_m = [\,\theta_1 \;\; \theta_2 \;\; \theta_3 \;\; \theta_4\,]^T$ is the joint angle column matrix.

The general dynamic equations of the tendon-actuated manipulator system can be described by Eq. (36). Because the mass matrix in Eq. (36) is symmetric, $\boldsymbol{M}_{r\omega}$ (3×3 matrix), $\boldsymbol{M}_{rm}$ (3×4 matrix) and $\boldsymbol{M}_{\omega m}$ (3×4 matrix) are equal to $\boldsymbol{M}_{\omega r}^T$ (3×3 matrix), $\boldsymbol{M}_{mr}^T$ (3×4 matrix) and $\boldsymbol{M}_{m\omega}^T$ (3×4 matrix), respectively. The expressions for the mass matrix are

$$\boldsymbol{M}_r = m\boldsymbol{I}_{3\times3} \tag{37}$$

$$\boldsymbol{M}_{\omega} = \boldsymbol{I}_t \tag{38}$$

$$\boldsymbol{M}_m = \begin{bmatrix} \boldsymbol{\eta}_1^T\boldsymbol{I}_{1t}\boldsymbol{\eta}_1 & \boldsymbol{\eta}_1^T\boldsymbol{A}_{12}\boldsymbol{I}_{2\_1}\boldsymbol{\eta}_2 & \boldsymbol{\eta}_1^T\boldsymbol{A}_{13}\boldsymbol{I}_{3\_1}\boldsymbol{\eta}_3 & \boldsymbol{\eta}_1^T\boldsymbol{A}_{14}\boldsymbol{I}_{4\_1}\boldsymbol{\eta}_4 \\ \boldsymbol{\eta}_2^T\boldsymbol{I}_{2\_1}^T\boldsymbol{A}_{21}\boldsymbol{\eta}_1 & \boldsymbol{\eta}_2^T\boldsymbol{I}_{2t}\boldsymbol{\eta}_2 & \boldsymbol{\eta}_2^T\boldsymbol{A}_{23}\boldsymbol{I}_{3\_2}\boldsymbol{\eta}_3 & \boldsymbol{\eta}_2^T\boldsymbol{A}_{24}\boldsymbol{I}_{4\_2}\boldsymbol{\eta}_4 \\ \boldsymbol{\eta}_3^T\boldsymbol{I}_{3\_1}^T\boldsymbol{A}_{31}\boldsymbol{\eta}_1 & \boldsymbol{\eta}_3^T\boldsymbol{I}_{3\_2}^T\boldsymbol{A}_{32}\boldsymbol{\eta}_2 & \boldsymbol{\eta}_3^T\boldsymbol{I}_{3t}\boldsymbol{\eta}_3 & \boldsymbol{\eta}_3^T\boldsymbol{A}_{34}\boldsymbol{I}_{4\_3}\boldsymbol{\eta}_4 \\ \boldsymbol{\eta}_4^T\boldsymbol{I}_{4\_1}^T\boldsymbol{A}_{41}\boldsymbol{\eta}_1 & \boldsymbol{\eta}_4^T\boldsymbol{I}_{4\_2}^T\boldsymbol{A}_{42}\boldsymbol{\eta}_2 & \boldsymbol{\eta}_4^T\boldsymbol{I}_{4\_3}^T\boldsymbol{A}_{43}\boldsymbol{\eta}_3 & \boldsymbol{\eta}_4^T\boldsymbol{I}_{4t}\boldsymbol{\eta}_4 \end{bmatrix} \tag{39}$$

$$\boldsymbol{M}_{r\omega} = -\boldsymbol{A}_{1b}\tilde{\boldsymbol{S}}_t \tag{40}$$

$$\boldsymbol{M}_{rm} = \begin{bmatrix} -\boldsymbol{A}_{11}\tilde{\boldsymbol{S}}_{1t}\boldsymbol{\eta}_1 & -\boldsymbol{A}_{12}\tilde{\boldsymbol{S}}_{2t}\boldsymbol{\eta}_2 & -\boldsymbol{A}_{13}\tilde{\boldsymbol{S}}_{3t}\boldsymbol{\eta}_3 & -\boldsymbol{A}_{14}\tilde{\boldsymbol{S}}_{4t}\boldsymbol{\eta}_4 \end{bmatrix} \tag{41}$$

$$\boldsymbol{M}_{\omega m} = \begin{bmatrix} \boldsymbol{A}_{b1}\boldsymbol{I}_{1\_o}\boldsymbol{\eta}_1 & \boldsymbol{A}_{b2}\boldsymbol{I}_{2\_o}\boldsymbol{\eta}_2 & \boldsymbol{A}_{b3}\boldsymbol{I}_{3\_o}\boldsymbol{\eta}_3 & \boldsymbol{A}_{b4}\boldsymbol{I}_{4\_o}\boldsymbol{\eta}_4 \end{bmatrix} \tag{42}$$

By considering the attitude motion of the central body spacecraft, substituting Eqs. (25) and (35) into Eq. (36) returns

$$\begin{bmatrix} \boldsymbol{M}_r & \boldsymbol{M}_{r\omega}\boldsymbol{H}_b & \boldsymbol{M}_{rm} \\ \boldsymbol{M}_{\omega r} & \boldsymbol{M}_{\omega}\boldsymbol{H}_b & \boldsymbol{M}_{\omega m} \\ \boldsymbol{M}_{mr} & \boldsymbol{M}_{m\omega}\boldsymbol{H}_b & \boldsymbol{M}_m \end{bmatrix} \begin{bmatrix} \ddot{\boldsymbol{r}}_b \\ \ddot{\boldsymbol{\Phi}}_b \\ \ddot{\boldsymbol{\theta}}_m \end{bmatrix} + \begin{bmatrix} \bar{\boldsymbol{F}}_{cr}^e \\ \bar{\boldsymbol{F}}_{c\omega}^e \\ \bar{\boldsymbol{F}}_{cm}^e \end{bmatrix} = \begin{bmatrix} \boldsymbol{F} \\ \boldsymbol{T} \\ \boldsymbol{D}\boldsymbol{x} \end{bmatrix} \tag{43}$$

where $\bar{\boldsymbol{F}}_{cr}^e$, $\bar{\boldsymbol{F}}_{c\omega}^e$ and $\bar{\boldsymbol{F}}_{cm}^e$ represent the new nonlinear coupled terms with the kinematical equations considered and are defined as follows

$$\bar{\boldsymbol{F}}_{cr}^e = \boldsymbol{F}_{cr}^e - \boldsymbol{A}_{1b}\tilde{\boldsymbol{S}}_t\boldsymbol{H}_{bc}\dot{\boldsymbol{\Phi}}_{bc} \tag{44}$$

$$\bar{\boldsymbol{F}}_{c\omega}^e = \boldsymbol{F}_{c\omega}^e + \boldsymbol{I}_t\boldsymbol{H}_{bc}\dot{\boldsymbol{\Phi}}_{bc} \tag{45}$$

$$\bar{\boldsymbol{F}}_{cm}^e = \boldsymbol{F}_{cm}^e + \boldsymbol{M}_{m\omega}\boldsymbol{H}_{bc}\dot{\boldsymbol{\Phi}}_{bc} \tag{46}$$

Eq. (43) represents the dynamic equations of the tendon-actuated manipulator system with the kinematics of the system and the relationship between the tensions and the equivalent joint actuated torque considered. According to Eq. (43), the dynamic equations of the tendon-actuated manipulator system are coupled. Considering that the timescale of the motion of the tendon-actuated manipulator is much smaller than the orbital period, the motion of the centroid of the central body spacecraft is neglected when designing the controller for the tendon-actuated manipulator system.

3. Controller design for the tendon-actuated manipulator system

In this section, firstly the attitude controller of the central body spacecraft and the trajectory tracking controller of the tendon-actuated manipulator are designed separately. Then, the tension analysis method is proposed, which is subject to the minimum and maximum allowable tensions in the cables. Finally, the characteristics of the actuators are analysed.

3.1. Attitude controller of the central body spacecraft

When the centroid motion of the central body spacecraft in Eq. (43) is neglected, a simplified dynamic model of the tendon-actuated manipulator system is obtained

$$\begin{bmatrix} \boldsymbol{M}_{\omega}\boldsymbol{H}_b & \boldsymbol{M}_{\omega m} \\ \boldsymbol{M}_{m\omega}\boldsymbol{H}_b & \boldsymbol{M}_m \end{bmatrix} \begin{bmatrix} \ddot{\boldsymbol{\Phi}}_b \\ \ddot{\boldsymbol{\theta}}_m \end{bmatrix} + \begin{bmatrix} \bar{\boldsymbol{F}}_{c\omega}^e \\ \bar{\boldsymbol{F}}_{cm}^e \end{bmatrix} = \begin{bmatrix} \boldsymbol{T} \\ \boldsymbol{T}_m \end{bmatrix} \tag{47}$$

Hence, the attitude motion equation of the central body spacecraft and the motion equation of the tendon-actuated manipulator are written as follows

$$\boldsymbol{M}_{\omega}\boldsymbol{H}_b\ddot{\boldsymbol{\Phi}}_b + \boldsymbol{M}_{\omega m}\ddot{\boldsymbol{\theta}}_m + \bar{\boldsymbol{F}}_{c\omega}^e = \boldsymbol{T} \tag{48}$$

$$\boldsymbol{M}_{m\omega}\boldsymbol{H}_b\ddot{\boldsymbol{\Phi}}_b + \boldsymbol{M}_m\ddot{\boldsymbol{\theta}}_m + \bar{\boldsymbol{F}}_{cm}^e = \boldsymbol{T}_m \tag{49}$$

The goal of designing the attitude controller of the central body spacecraft is to stabilise its attitude relative to the earth. Hence, the control torque of the central body spacecraft is designed as follows

$$\boldsymbol{T} = \bar{\boldsymbol{F}}_{c\omega}^e + \boldsymbol{T}_{bf} + \boldsymbol{T}_{bc} \tag{50}$$

where $\boldsymbol{T}_{bf}$ is the attitude feedback control torque, and $\boldsymbol{T}_{bc}$ is the compensation torque of the tendon-actuated manipulator. Define the attitude angle error as

$$\Delta\boldsymbol{\Phi}_b = \boldsymbol{\Phi}_b - \boldsymbol{\Phi}_b^d \tag{51}$$

where $\boldsymbol{\Phi}_b^d$ is the desired attitude angle of the central body spacecraft. Therefore, the attitude feedback control torque is designed as

$$\boldsymbol{T}_{bf} = \boldsymbol{M}_{\omega}\boldsymbol{H}_b\left(\ddot{\boldsymbol{\Phi}}_b^d - \boldsymbol{K}_{pbf}\Delta\boldsymbol{\Phi}_b - \boldsymbol{K}_{dbf}\Delta\dot{\boldsymbol{\Phi}}_b\right) \tag{52}$$

where $\boldsymbol{\Phi}_b^d$, $\dot{\boldsymbol{\Phi}}_b^d$ and $\ddot{\boldsymbol{\Phi}}_b^d$ are equal to $\boldsymbol{0}$ because the attitude of the central body spacecraft is required to be stable relative to the earth. $\boldsymbol{K}_{pbf}$ and $\boldsymbol{K}_{dbf}$ are the proportional and the differential coefficients, respectively. They are all chosen as positive diagonal matrix.

The motion of the tendon-actuated manipulator alters the attitude of the central body spacecraft, as shown in Eq. (48), and the effects of the tendon-actuated manipulator therefore can be equivalently regarded as changing the angular momentum of the central body spacecraft. Hence, properly compensating the angular momentum of the central body spacecraft can help eliminate the effects of the tendon-actuated manipulator. Assuming that the angular momentum corresponding to the compensation torque $\boldsymbol{T}_{bc}$ is $\boldsymbol{h}_b$, the relation between them is given by

$$\dot{\boldsymbol{h}}_b = \boldsymbol{T}_{bc} \tag{53}$$

Define the angular momentum error of the central body spacecraft as

$$\Delta \boldsymbol{h}_b = \boldsymbol{h}_b - \boldsymbol{h}_b^d \tag{54}$$

where $\boldsymbol{h}_b^d$ is the desired compensation angular momentum and is approximately given by

$$\boldsymbol{h}_b^d = \boldsymbol{M}_{\omega m}\dot{\boldsymbol{\theta}}_m \tag{55}$$

Therefore, the compensation torque of the tendon-actuated manipulator is designed as

$$\boldsymbol{T}_{bc} = -\boldsymbol{K}_{pbc}\Delta \boldsymbol{h}_b - \boldsymbol{K}_{ibc}\int \Delta \boldsymbol{h}_b dt \tag{56}$$

where $\boldsymbol{K}_{pbc}$ and $\boldsymbol{K}_{ibc}$ are the proportional and the integral coefficients, respectively. They are all chosen as positive diagonal matrix.

3.2. Trajectory tracking controller for the tendon-actuated manipulator

The goal of designing the controller for the tendon-actuated manipulator is to track the desired trajectory of the endpoint. Therefore, the equivalent joint actuated torque is designed as follows

$$\boldsymbol{T}_m = \bar{\boldsymbol{F}}_{cm}^e + \boldsymbol{T}_{mf} + \boldsymbol{T}_{mc} \tag{57}$$

where $\boldsymbol{T}_{mf}$ is the trajectory tracking control torque, and $\boldsymbol{T}_{mc}$ is the compensation torque of the central body spacecraft. Define the joint angle error as

$$\Delta \boldsymbol{\theta}_m = \boldsymbol{\theta}_m - \boldsymbol{\theta}_m^d \tag{58}$$

where $\boldsymbol{\theta}_m^d$ is the desired joint angle vector of the tendon-actuated manipulator. Therefore, the trajectory tracking control torque is designed as

$$\boldsymbol{T}_{mf} = \boldsymbol{M}_m\left(\ddot{\boldsymbol{\theta}}_m^d - \boldsymbol{K}_{pmf}\Delta \boldsymbol{\theta}_m - \boldsymbol{K}_{dmf}\Delta \dot{\boldsymbol{\theta}}_m\right) \tag{59}$$

where $\boldsymbol{K}_{pmf}$ and $\boldsymbol{K}_{dmf}$ are the proportional and the differential coefficients, respectively. They are all chosen as positive diagonal matrix. $\boldsymbol{\theta}_m^d$, $\dot{\boldsymbol{\theta}}_m^d$ and $\ddot{\boldsymbol{\theta}}_m^d$ can be obtained from the trajectory planning of the tendon-actuated manipulator.

Similarly, the compensation torque of the central body spacecraft is designed as

$$\boldsymbol{T}_{mc} = -\boldsymbol{K}_{pmc}\Delta \boldsymbol{h}_m - \boldsymbol{K}_{imc}\int \Delta \boldsymbol{h}_m dt \tag{60}$$

where $\Delta \boldsymbol{h}_m$ is the angular momentum error of the tendon-actuated manipulator. $\boldsymbol{K}_{pmc}$ and $\boldsymbol{K}_{imc}$ are the proportional and the integral coefficients, respectively. They are all chosen as positive diagonal matrix.

3.3. Tension analysis

The equivalent joint actuated torque is given by Eq. (57), but the joint actuated torque is produced by the tensions in the cables. Hence, a method of evaluating the tensions from the equivalent joint actuated torque is proposed. The relationship between the equivalent joint actuated torque and the tensions in the cables is shown in Eq. (35), where the matrix $\boldsymbol{D}$ is given by

$$\boldsymbol{D} = \begin{bmatrix} f_-(\theta_1) & -f_+(\theta_1) & 0 & 0 & 0 & 0 & 0 & 0 \\ 0 & 0 & f_-(\theta_2) & -f_+(\theta_2) & 0 & 0 & 0 & 0 \\ 0 & 0 & 0 & 0 & f_-(\theta_3) & -f_+(\theta_3) & 0 & 0 \\ 0 & 0 & 0 & 0 & 0 & 0 & f_-(\theta_4) & -f_+(\theta_4) \end{bmatrix} \tag{61}$$

where

$$f_-(\theta_i) = \frac{Ld\cos\frac{\theta_i}{2}}{2\sqrt{L^2 + \frac{d^2}{4} - Ld\sin\frac{\theta_i}{2}}},$$
$$f_+(\theta_i) = \frac{Ld\cos\frac{\theta_i}{2}}{2\sqrt{L^2 + \frac{d^2}{4} + Ld\sin\frac{\theta_i}{2}}} \tag{62}$$

The tensions in the cables can be obtained by solving Eq. (35), but the number of results is infinite. Therefore, the tensions can be evaluated based on the pseudo inverse of matrix $\boldsymbol{D}$:

$$\boldsymbol{x} = \boldsymbol{D}^+\boldsymbol{T}_m + \alpha\left(\boldsymbol{I}_{8\times 8} - \boldsymbol{D}^+\boldsymbol{D}\right)\boldsymbol{\delta} \tag{63}$$

where $\boldsymbol{D}^+$ is the pseudo inverse of $\boldsymbol{D}$, and $\boldsymbol{D}^+ = \boldsymbol{D}^T(\boldsymbol{D}\boldsymbol{D}^T)^{-1}$; α is a parameter, and $\boldsymbol{I}_{8\times 8}$ is an 8×8 unit matrix; and $\boldsymbol{\delta}$ is the vector in null space that is to be designed. The second term on the right of Eq. (63) represents the adjustable part of the tensions, and it will not change the equivalent joint actuated torque. Considering the practical working condition of the cables, the tensions must be limited between the minimum and maximum values. The minimum value limit ensures that the cables are in tension, and the maximum value limit ensures that the tensions in the cables are always smaller than the allowable tension. Let $\sigma_{\min}$ and $\sigma_{\max}$ represent the minimum allowable tension and the maximum allowable tension, respectively. Hence, adjusting α and $\boldsymbol{\delta}$ can satisfy the tension constraint. Define a function to describe the distribution of the tensions:

$$L(\boldsymbol{x}) = \frac{1}{8}\begin{bmatrix} 1 & \dots & 1 \end{bmatrix}\boldsymbol{x} \tag{64}$$

where $L(\boldsymbol{x})$ is the average of the tensions. Letting $\boldsymbol{\beta} = \frac{1}{8}\begin{bmatrix} 1 & \dots & 1 \end{bmatrix}^T$, $L(\boldsymbol{x}) = \boldsymbol{\beta}^T\boldsymbol{x}$.

Substituting Eq. (63) into Eq. (64) returns

$$L(\boldsymbol{x}) = \boldsymbol{\beta}^T\boldsymbol{D}^+\boldsymbol{T}_m + \alpha\boldsymbol{\beta}^T\left(\boldsymbol{I}_{8\times 8} - \boldsymbol{D}^+\boldsymbol{D}\right)\boldsymbol{\delta} \tag{65}$$

From Eq. (65), it can be determined that the way to change the average of the tensions is only by adjusting the second term on the right. Let $L_n(\boldsymbol{x})$ represent the second term:

$$L_n(\boldsymbol{x}) = \alpha\boldsymbol{\beta}^T\left(\boldsymbol{I}_{8\times 8} - \boldsymbol{D}^+\boldsymbol{D}\right)\boldsymbol{\delta} \tag{66}$$

Define a new vector $\boldsymbol{\gamma}$ as

$$\boldsymbol{\gamma} = \left[\boldsymbol{\beta}^T\left(\boldsymbol{I}_{8\times 8} - \boldsymbol{D}^+\boldsymbol{D}\right)\right]^T \tag{67}$$

Then, $L_n(\boldsymbol{x})$ can be rewritten as

$$L_n(\boldsymbol{x}) = \alpha\boldsymbol{\gamma}^T\boldsymbol{\delta} \tag{68}$$

The purpose of designing α and $\boldsymbol{\delta}$ is to obtain the suitable average of the tensions so that the tensions in the cables always vary between the minimum and maximum values. Therefore, the vector $\boldsymbol{\delta}$ can be designed as

$$\boldsymbol{\delta} = \frac{\boldsymbol{\gamma}}{\boldsymbol{\gamma}^T\boldsymbol{\gamma}} \tag{69}$$

Choosing parameter α can then change the mean tension since the average of the tensions is equal to α.

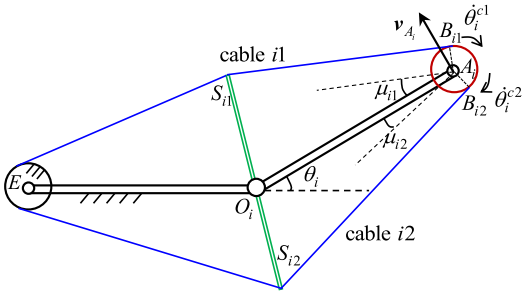

Fig. 7. Kinematical relation of the actuators. (For interpretation of the colours in the figure(s), the reader is referred to the web version of this article.)

3.4. Actuator analysis

The actuated motors of the tendon-actuated manipulator are equipped on the right end of every link so that they can drive the capstans to reel cable in or out, which is shown in Fig. 7. The red circle in Fig. 7 represents the two different capstans, where the two capstans coincide. $\dot{\theta}_i^{c1}$ and $\dot{\theta}_i^{c2}$ represent the angular velocities of the capstans for the cables $i1$ and the cable $i2$, respectively. That is to say, the two different capstans can independently control the cable $i1$ and the cable $i2$. When the right link rotates around the left link, the length of the cable $i1$ will increase (or decrease), and meanwhile, the length of the cable $i2$ will correspondingly decrease (or increase). Hence, one of the capstans will reel cable in, and the other will reel cable out. The capstan $i1$ is chosen as an example to illustrate the equations of motion of the capstans. Neglecting the friction between the cable $i1$ and the capstan $i1$, then the motion of the capstan $i1$ can be described as follows

$$J_i^{c1}\ddot{\theta}_i^{c1} = T_i^{c1} - N_i^{c1}R \tag{70}$$

where J_i^{c1} is the moment of inertia of the capstan $i1$; T_i^{c1} is the actuated torque of the capstan $i1$, and it equals to the output torque of the motor; R is the radius of the capstans.

The angular velocities of the capstans are related to the angular velocity of the corresponding joint. As is shown in Fig. 7, B_{i1} is the point of tangency between the cable $i1$ and the capstan $i1$, and B_{i2} is the point of tangency between the cable $i2$ and the capstan $i2$. Then, the velocity vector of B_{i1} is calculated as follows

$$\boldsymbol{v}_{B_{i1}} = \boldsymbol{v}_{A_i} + \left(\dot{\theta}_i^{c1}\boldsymbol{k}_i^{c1}\right) \times \left(R\boldsymbol{n}_i^{c1}\right) \tag{71}$$

where $\boldsymbol{v}_{A_i}$ represents the velocity vector of the end point of the right link; $\boldsymbol{k}_i^{c1}$ represents the rotational direction of the capstan $i1$; $\boldsymbol{n}_i^{c1}$ is the unit vector that points from A_i to B_{i1}. Since the cable $i1$ is fixed on the left side, the velocity component of B_{i1} along the tangent line is equal to zero. Therefore, the angular velocity of the capstan $i1$ is obtained by projecting Eq. (71) along the tangent line:

$$\dot{\theta}_i^{c1} = \frac{L}{R}\dot{\theta}_i \sin\mu_{i1} \tag{72}$$

where μ_{i1} is the angle between the right link and the cable $i1$, which satisfies the following relationship

$$\sin\mu_{i1} = \frac{d\sqrt{L^2 + \frac{d^2}{4} - R^2 - Ld\sin\frac{\theta_i}{2}}\cos\frac{\theta_i}{2} + Rd\sin\frac{\theta_i}{2} - 2RL}{2(L^2 + \frac{d^2}{4} - Ld\sin\frac{\theta_i}{2})} \tag{73}$$

Differentiating Eq. (72) with respect to time returns

$$\ddot{\theta}_i^{c1} = \frac{L}{R}\ddot{\theta}_i \sin\mu_{i1} + \frac{L}{R}\frac{d\sin\mu_{i1}}{d\theta_i}\dot{\theta}_i^2 \tag{74}$$

Eq. (74) indicates that the angular acceleration of the capstan $i1$ is determined by the joint angle θ_i, the joint angular velocity $\dot{\theta}_i$ and the joint angular acceleration $\ddot{\theta}_i$. Substituting Eqs. (63) and (74) into Eq. (70), the actuated torque of the capstan $i1$ is obtained. Similarly, the actuated torques of the other capstans can be determined.

Fig. 8 gives the block diagram of the control system of the tendon-actuated manipulator system, which contains the attitude controller of the central body spacecraft and the trajectory tracking controller of the tendon-actuated manipulator. The control methods of the central body spacecraft and the tendon-actuated manipulator are very similar. Due to the dynamic equations of the tendon-actuated manipulator are coupled, the motion of the manipulator has influence on the attitude motion of the central body spacecraft, meanwhile, the attitude motion of the central body spacecraft also has influence on the motion of the manipulator. Therefore, when stabilise the attitude of the central body spacecraft, the motion of the manipulator can be compensated by a PI

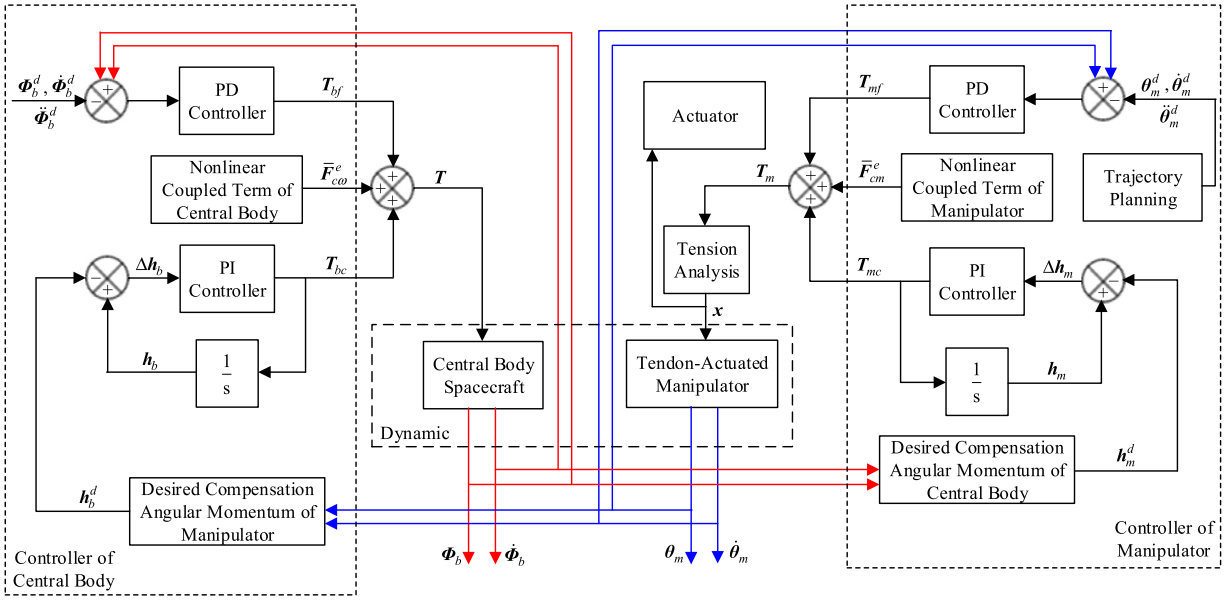

Fig. 8. Block diagram of the control system.

Table 1
Parameters of the short link, tendon-actuated manipulator system.

Object	Mass/(kg)	First moment/(kg m)	Moment of inertia/(kg m^2)
Central body spacecraft	4500	$[0\ 0\ 0]^T$	*diag*(6891 12820 12820)
Link	7.5	$[11.25\ 0\ 0]^T$	*diag*(0.0125 22.5063 22.5063)
Spreader	1.5	$[0\ 0\ 0]^T$	*diag*(0.18125 0.18 0.00133)

controller. In other words, the disturbance of the manipulator to the central body spacecraft can be eliminated by the PI controller. That is to say, not only the attitude angle and the angular velocity of the central body spacecraft, but also the joint angle and the joint angular velocity of the tendon-actuated manipulator are required to control the attitude of the central body spacecraft. The characteristics of the trajectory tracking controller of the tendon-actuated manipulator are same as the attitude controller of the central body spacecraft discussed above.

4. Numerical simulations

In this section, two simulation examples are given based on different structural parameters of the tendon-actuated manipulator system. The greatest difference is the length of the links and spreaders, and the goal of controlling the tendon-actuated manipulator is to let the endpoint track a circular trajectory described in the body fixed frame of the central body spacecraft.

4.1. Short links

Assume that the central body spacecraft is a cylinder with a length 5 m and a diameter of 3.5 m. The four links have lengths of 3 m, and the spreaders have lengths of 1.2 m. Therefore, the links and spreaders are each identical. The physical properties of the tendon-actuated manipulator system (masses, first moments and moments of inertia) are shown in Table 1. In addition, the radius of the capstans are 0.1 m. The minimum allowable tension is $\sigma_{\min} = 20$ N, and the maximum allowable tension is $\sigma_{\max} = 300$ N. The value of the chosen α parameter is 40.

The initial attitude angle of the central body spacecraft is $\boldsymbol{\Phi}_{b0} = \left[\ 2^\circ\ \ -2^\circ\ \ 3^\circ\ \right]^T$, and the initial angular velocity of the central body spacecraft is zero. The central body spacecraft is required to maintain attitude stability when the tendon-actuated manipulator is in operation, and the desired attitude angle is therefore $\boldsymbol{\Phi}_b^d = \left[\ 0\ \ 0\ \ 0\ \right]^T$. For the tendon-actuated manipulator, the initial joint angle is $\boldsymbol{\theta}_{m0} = \left[\ 0.4\ \ 0.5\ \ -0.4\ \ -0.5\ \right]^T$ rad, and the corresponding position of the endpoint is $\boldsymbol{r}_{e0} = \left[\ 13.3710\ \ 2.2147\ \ -4.2134\ \right]^T$ m. The centre of the circular trajectory is $\boldsymbol{r}_{ec} = \left[\ 9.5\ \ 2.5\ \ -1\ \right]^T$ m, and the radius of the circular trajectory is therefore 5.039 m.

Figs. 9–22 show the results of the endpoint tracking of a circular trajectory for 250 s. The reason why all the variables change by somewhat large amounts near 100 s is that the velocity of the endpoint reaches the maximum value so that the joint angular velocity reaches its maximum value simultaneously. Considering the coupling characteristics between the central body spacecraft and the tendon-actuated manipulator, the attitude motion will be affected by the motion of the tendon-actuated manipulator such that the attitude angle, the angular velocity and the control torque of the central body spacecraft change was somewhat great near 100 s. Fig. 12 depicts the joint angle error of tracking the desired joint angle shown in Fig. 11. The maximum tracking error of the joint angle is approximately 0.03°. Figs. 13 and 14 show the control torque of the central body spacecraft and the equivalent joint actuated torque of the tendon-actuated manipulator, respectively.

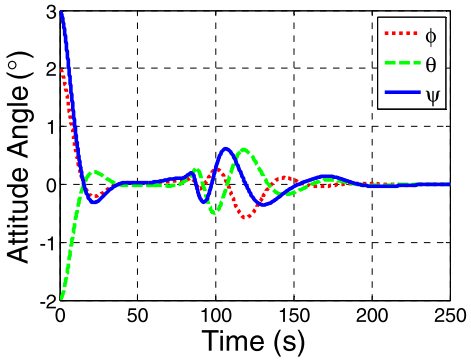

Fig. 9. Attitude angle of the central body.

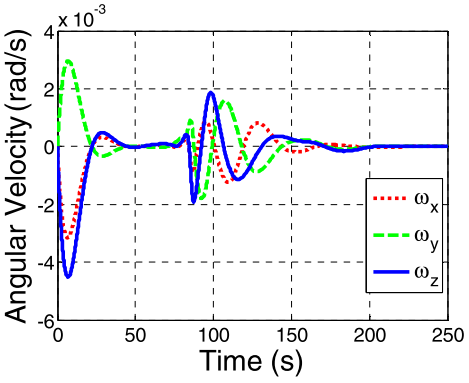

Fig. 10. Angular velocity of the central body.

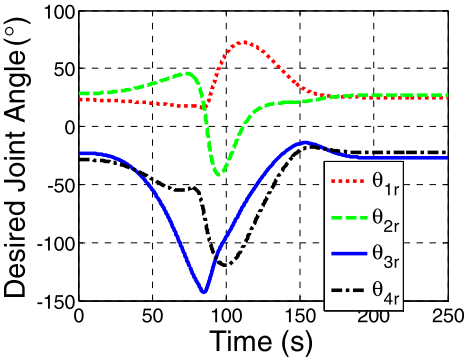

Fig. 11. Desired joint angles of the manipulator.

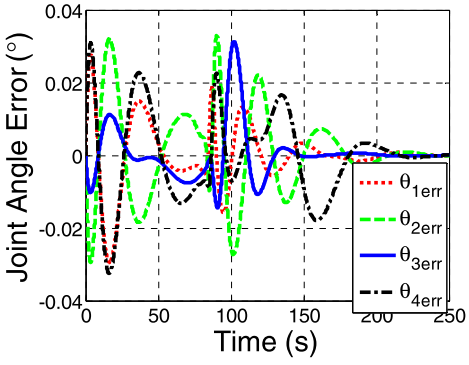

Fig. 12. Joint angle errors of the manipulator.

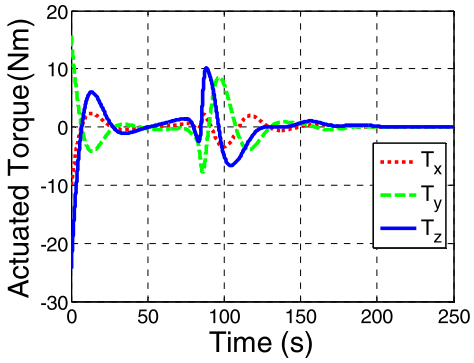

Fig. 13. Control torques of the central body.

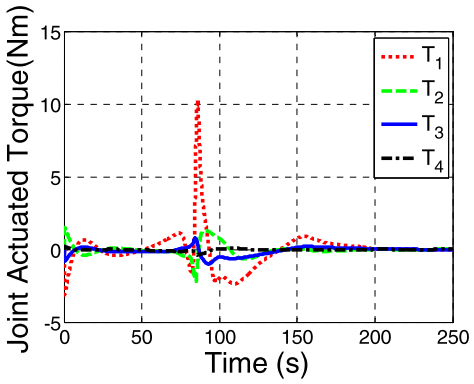

Fig. 14. Control torques of the manipulator.

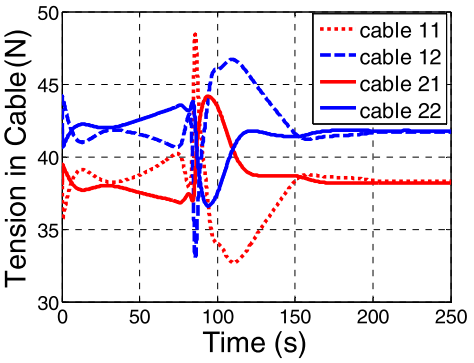

Fig. 15. Tensions in the cables around joints 1 and 2.

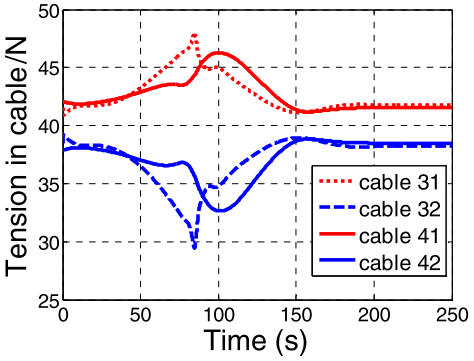

Fig. 16. Tensions in the cables around joints 3 and 4.

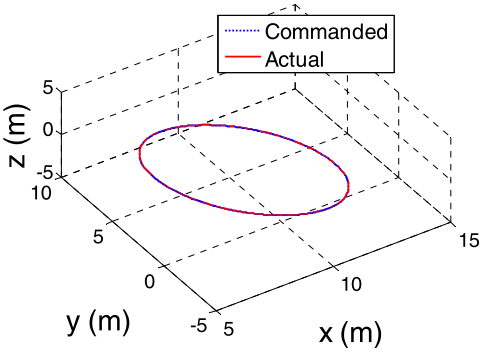

Fig. 17. Trajectory of the endpoint.

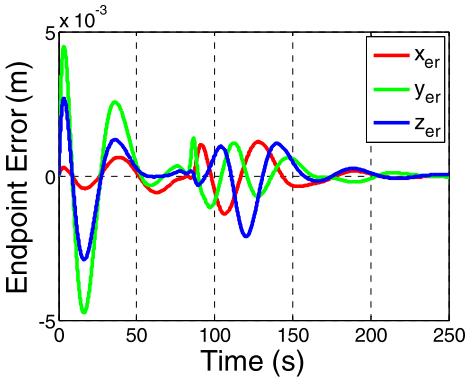

Fig. 18. Tracking errors of the endpoint.

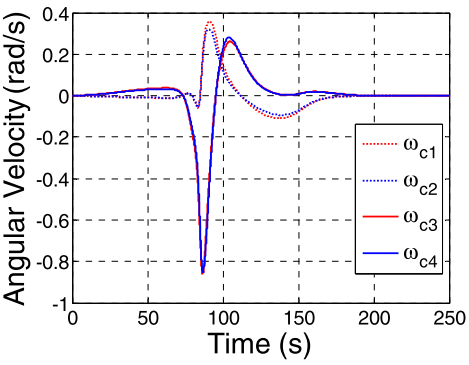

Fig. 19. Angular velocities of capstans 1–4.

Because the length of the links is small, causing the moment of inertia to also be small, the equivalent joint actuated torque is also very small. Figs. 15 and 16 indicate that the two tensions around one joint change symmetrically due to the symmetry of the structure of the tendon-actuated manipulator. Fig. 18 depicts the three position component errors of the endpoint while tracking the circular trajectory described in the central body coordinate system that is shown in Fig. 17. The maximum trajectory tracking error of the endpoint is less than 5 mm because the maximum joint angle error is approximately 0.03°. Figs. 19 and 20 depict the variations in time of the angular velocities of the capstans. When the velocity of the endpoint approaches the maximum value, the changes in the angular velocities of the capstans are very large. However, the trends of the angular velocities of the two capstans related to one joint are almost the same. In addition, the maximum angular velocities of the capstans are below 0.9 rad/s. Figs. 21 and 22 depict the required actuated torques acting on the capstans, which can be provided by the actuated motors located at the ends of the links.

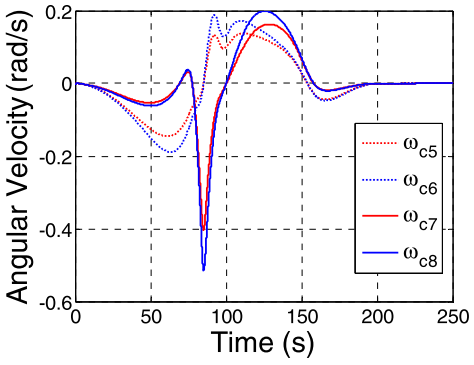

Fig. 20. Angular velocities of capstans 5–8.

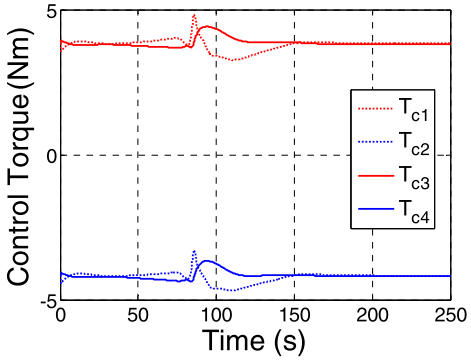

Fig. 21. Actuated torques of capstans 1–4.

The results show that the variation range of the actuated torques of the capstans is relative small, and the trends of the actuated torques of the two capstans around one joint are almost the same. According to Figs. 14 and 21–22, the differences between the capstans' actuated torques and the equivalent joint actuated torques are small, which means that when setting the actuated motors in the joint and in the end of the links, respectively, the differences between the required output torques of the motors are small.

4.2. Long links

This part provides a simulation example that features long links in the tendon-actuated manipulator, where the central body spacecraft is the same as that previous. The length of the links is 30 m, and the length of the spreaders is 12 m. Table 2 shows the masses, first moments and moments of inertia of the tendon-actuated manipulator system components. The initial attitude angle of the central body spacecraft is $\boldsymbol{\Phi}_{b0} = \left[\, 2^\circ \;\; -2^\circ \;\; 3^\circ \,\right]^T$, and the initial angular velocity of the central body spacecraft is zero. The desired attitude angle is $\boldsymbol{\Phi}_b^d = \left[\, 0 \;\; 0 \;\; 0 \,\right]^T$. For the tendon-actuated manipulator, the initial joint angle is $\boldsymbol{\theta}_{m0} = \left[\, 0.4 \;\; 0.5 \;\; -0.4 \;\; -0.5 \,\right]^T$ rad, and the corresponding position of the endpoint is $\boldsymbol{r}_{e0} = \left[\, 111.2099 \;\; 22.1469 \;\; -28.1838 \,\right]^T$ m. The centre of the circular trajectory is $\boldsymbol{r}_{ec} = \left[\, 80 \;\; 10 \;\; 10 \,\right]^T$ m, and therefore the radius of the circular trajectory is 50.7898 m. In addition, the radii of the capstans are 0.2 m. The minimum allowable tension is $\sigma_{\min} = 20$ N, and the maximum allowable tension is $\sigma_{\max} = 300$ N. The parameter α is chosen as 120.

Figs. 23–36 show the results of the endpoint tracking a circular trajectory in 500 s. From Figs. 14 and 28, the equivalent joint actuated torques in the long links are approximately one hundred times those in the short links given that the moments of inertia of the long links are much larger than for the short links. In addition, considering the coupling characteristics, the control torques of the central body spacecraft are also very large. In addition, the ranges in variations in attitude angle, angular velocity of the central body spacecraft and joint angle tracking error, the tensions in the cables and the trajectory tracking errors of the endpoint are relative large. Fig. 26 shows that the maximum joint angle tracking error is approximately 2°, which causes the maximum position component errors of the endpoint tracking on the circular trajectory shown in Fig. 31 to be less than 1 m, as shown in Fig. 32. Although the equivalent joint actuated torques in the long links are approximately one hundred times those in short links, the tensions in the cables in the long links are approximately five times

Table 2
Parameters of the tendon-actuated manipulator system with long links.

Object	Mass/(kg)	First moment/(kg m)	Moment of inertia/(kg m^2)
Link	75	$[1125\ 0\ 0]^T$	*diag*(3.125 22500 22500)
Spreader	15	$[0\ 0\ 0]^T$	*diag*(180 180 0.3906)

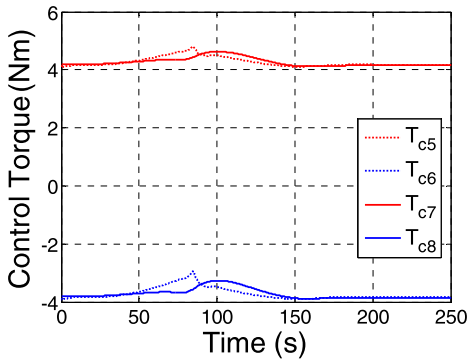

Fig. 22. Actuated torques of capstans 5–8.

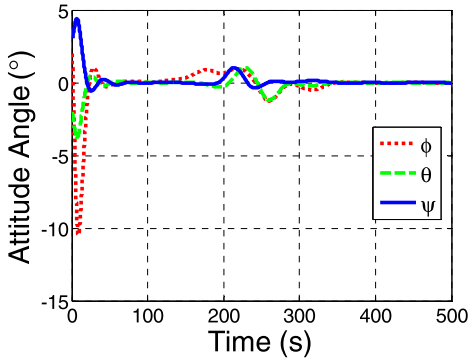

Fig. 23. Attitude angles of the central body.

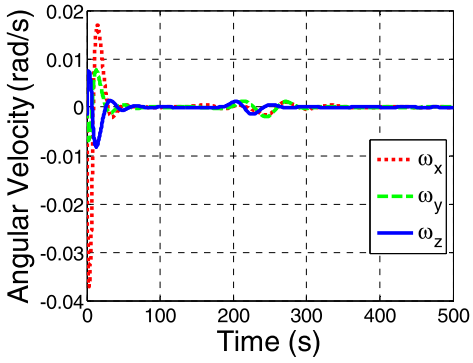

Fig. 24. Angular velocity of the central body.

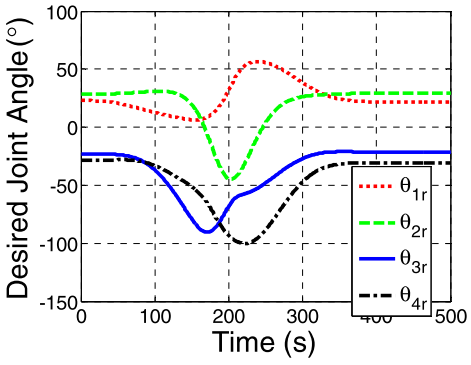

Fig. 25. Desired joint angles of the manipulator.

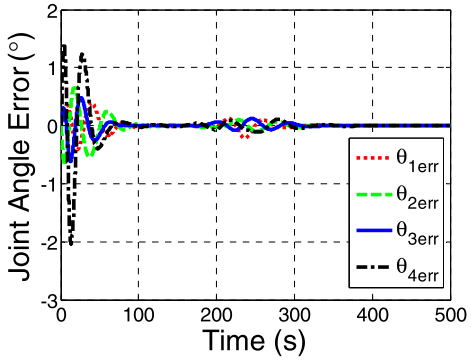

Fig. 26. Joint angle errors of the manipulator.

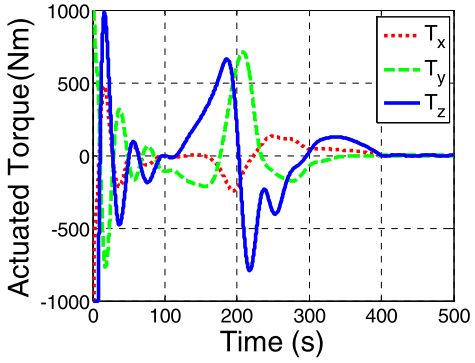

Fig. 27. Control torques of the central body.

those in the short links, and the actuated torques of the capstans in the long links are approximately ten times those in the short links. Figs. 33 and 34 depict the variations over time in the angular velocities of the capstans, and the maximum angular velocity is still less than 0.9 rad/s. From Figs. 29 and 30, the two tensions around one joint still change symmetrically. From Figs. 33–36, the trends in the angular velocities and the actuated torques of the two capstans related to one joint are almost the same. According to Figs. 28 and 35–36, the equivalent joint actuated torques are approximately twenty-five times those of the actuated torques of the capstans. This means that the output torques of the actuated motors will decrease greatly when setting the actuated motors at the ends of the links instead of in the joint.

When the lengths of the links increase, the moment of inertia of the links increases greatly so that the required equivalent joint actuated torque will increase greatly simultaneously. Therefore, the effects of the coupling characteristics between the central body spacecraft and the tendon-actuated manipulator become more obvious. Comparing the tensions and the equivalent joint ac-

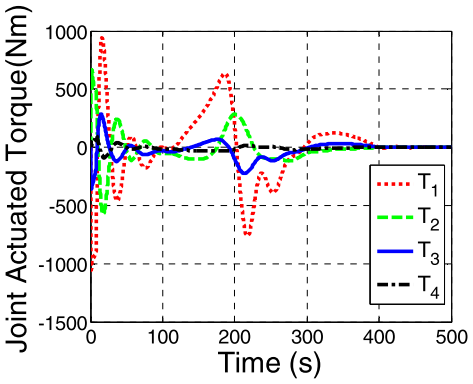

Fig. 28. Control torques of the manipulator.

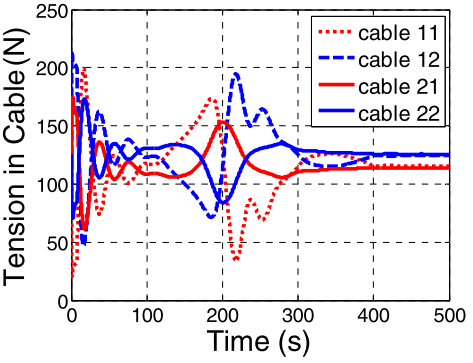

Fig. 29. Tensions in the cables around joints 1 and 2.

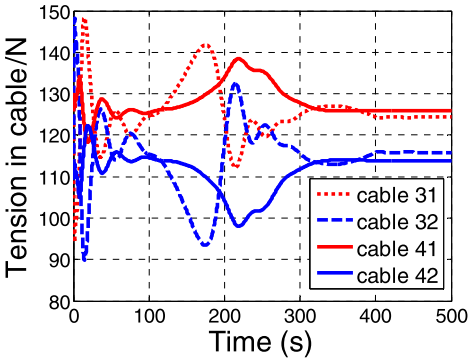

Fig. 30. Tensions in the cable around joints 3 and 4.

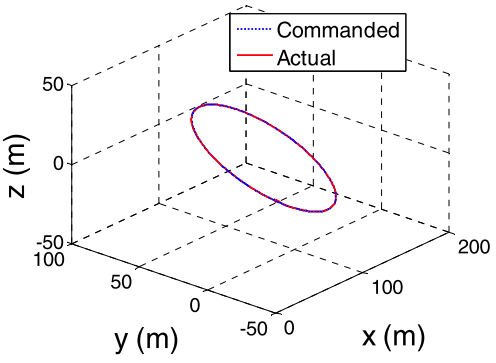

Fig. 31. Trajectory of the endpoint.

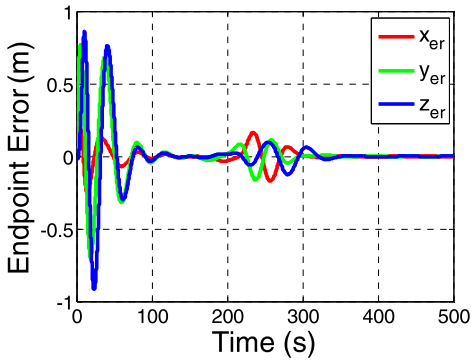

Fig. 32. Tracking errors of the endpoint.

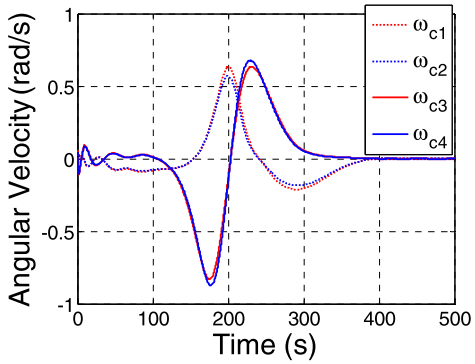

Fig. 33. Angular velocities of capstans 1–4.

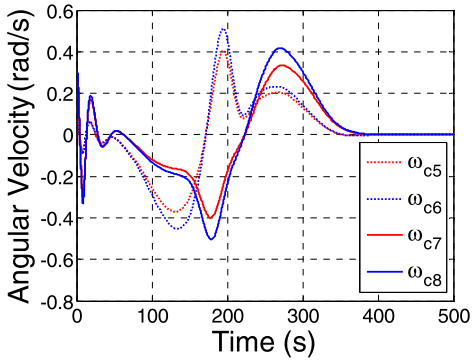

Fig. 34. Angular velocities of capstans 5–8.

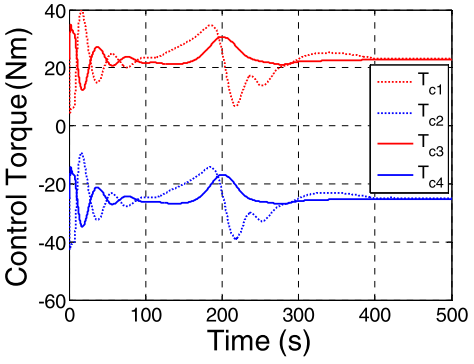

Fig. 35. Actuated torques of capstans 1–4.

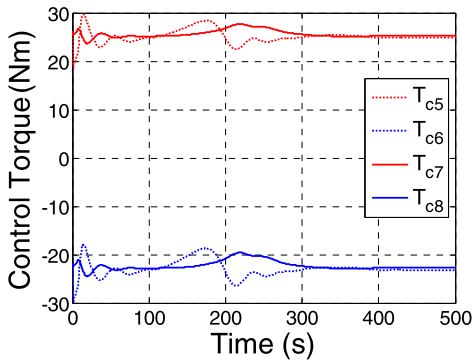

Fig. 36. Actuated torques of capstans 5–8.

tuated torques in the short links and long links, the changes in the tensions are much smaller than the actuated torques. In addition, comparing the actuated torques of the capstans and the equivalent joint actuated torques in the short links and long links, the changes in the actuated torques of the capstans are also much smaller than the equivalent joint actuated torques. Hence, the advantages of the long link, tendon-actuated manipulator are much more obvious than those of the long link conventional manipulators.

5. Conclusions

This paper has discussed the dynamic modelling and control of a four-degree-of-freedom Tendon-Actuated Lightweight Space Manipulator mounted on a central body spacecraft. The dynamic equations of the tendon-actuated manipulator system are coupled, which means that the translation of the central body spacecraft, the rotation of the central body spacecraft and the rotation of the links can affect each other. The attitude motion of the central body spacecraft will be affected by the motion of the links much more greatly with increasing mass and moment of inertia of the links. Compared with conventional space manipulators, the required output torques of the actuated motors in the tendon-actuated manipulator are much smaller, especially for long links. The cables in the tendon-actuated manipulator can enlarge the joint actuated torque owing to the tensions in the cables and can reduce the required output torques of the actuated motors, resulting in reductions in the mass and size of the actuators. The tensions in the cables change almost symmetrically around the average of the tensions, and the values of the tensions are acceptable for practical working conditions. The tendon-actuated manipulator is more suitable for missions requiring large ranges of motion when compared to conventional space manipulators. The simulations illustrate the merits of the long links, tendon-actuated manipulator.

Conflict of interest statement

There is no conflict of interest.

Acknowledgement

This study was supported by the National Natural Science Foundation of China (No. 11672035).

References

[1] F. Feng, L. Tang, J. Xu, H. Liu, Y. Liu, A review of the end-effector of large space manipulator with capabilities of misalignment tolerance and soft capture, Sci. China, Technol. Sci. 59 (11) (2016) 1621–1638.
[2] S. Aziz, Lessons learned from the STS-120/ISS 10A robotics operations, Acta Astronaut. 66 (2010) 157–165.

[3] P. Laryssa, E. Lindsay, O. Layi, et al., International space station robotics: a comparative study of ERA, JEMRMS and MSS, in: 7th ESA Workshop on Advanced Space Technologies for Robotics and Automation, ASTRA 2002, Noordwijk, the Netherlands, Nov. 19–21, 2002.
[4] G. Hirzinger, K. Landzettel, B. Brunner, et al., DLR's robotics technologies for on-orbit servicing, Adv. Robot. 18 (2) (2004) 139–174.
[5] E.E. Komendera, W.R. Doggett, J.T. Dorsey, et al., Control system design implementation and preliminary demonstration for a Tendon-Actuated Lightweight In-Space MANipulator (TALISMAN), in: AIAA SPACE 2015 Conference and Exposition, Pasadena, CA, USA, Aug. 31–Sep. 2, 2015, AIAA 2015-4628.
[6] W.R. Doggett, J.T. Dorsey, G.G. Ganoe, Tension Stiffened and Tendon Actuated Manipulator, United States Patent, National Aeronautics and Space Administration, Washington, DC, USA, No. US9168659B2, filed Apr. 17, 2013.
[7] J.T. Dorsey, W.R. Doggett, T.C. Jones, B. King, Application of a novel long-reach manipulator concept to asteroid redirect missions, in: 2nd AIAA Spacecraft Structures Conference, Kissimmee, FL, USA, Jan. 5–9, 2015, AIAA 2015-0225.
[8] W.R. Doggett, J.T. Dorsey, T.C. Jones, B. King, Development of a Tendon-Actuated Lightweight In-Space MANipulator (TALISMAN), in: Proceedings of the 42nd Aerospace Mechanisms Symposium, Baltimore, MD, USA, May 14–16, 2014, pp. 405–420.
[9] W.R. Doggett, J.T. Dorsey, T.C. Jones, et al., Improvements to the Tendon-Actuated Lightweight In-Space MANipulator (TALISMAN), in: AIAA SPACE 2015 Conference and Exposition, Pasadena, CA, USA, Aug. 31–Sep. 2, 2015, AIAA 2015-4682.
[10] C. Altenbuchner, Flexible multi-body dynamic modeling of a Tendon-Actuated Lightweight In-Space MANipulator (TALISMAN), in: AIAA SPACE 2015 Conference and Exposition, Pasadena, CA, USA, Aug. 31–Sep. 2, 2015, AIAA 2015-4629.
[11] C. Altenbuchner, Dynamic response characteristics of a robotic manipulator-based capture system performing the asteroid redirect mission, in: AIAA SPACE 2015 Conference and Exposition, Pasadena, CA, USA, Aug. 31–Sep. 2, 2015, AIAA 2015-4630.
[12] C.W. de Silva, Trajectory design for robotic manipulators in space applications, J. Guid. Control Dyn. 14 (3) (1971) 670–674.
[13] T. Iwata, Y. Toda, K. Machida, Dynamic control of free flying robot for capturing maneuvers, in: Navigation and Control Conference, Guidance, Navigation, and Control and Co-Located Conferences, New Orleans, LA, USA, Aug. 12–14, 1991, AIAA 1991-2824-CP.
[14] E. Stoneking, Newton–Euler dynamic equations of motion for a multi-body spacecraft, in: AIAA Guidance, Navigation and Control Conference and Exhibit, Hilton Head, CA, USA, Aug. 20–23, 2007, AIAA 2007-6441.
[15] V. Aslanov, G. Kruglov, V. Yudintsev, Newton–Euler equations of multibody systems with changing structures for space applications, Acta Astronaut. 68 (2011) 2080–2087.
[16] A. Pisculli, L. Felicetti, P. Gasbarri, G.B. Palmerini, M. Sabatini, A reaction-null/Jacobian transpose control strategy with gravity gradient compensation for on-orbit space manipulators, Aerosp. Sci. Technol. 38 (2014) 30–40.
[17] D. Tan, Dynamic simulations of space manipulators with flexible links, in: 54th International Astronautical Congress, Bremen, Germany, Sep. 29–Oct. 3, 2003.
[18] S. Ali, A. Moosavian, E. Papadopoulos, Explicit dynamics of space free-flyers with multiple manipulators via SPACEMAPLE, Adv. Robot. 18 (2) (2004) 223–244.
[19] Z. Zhou, Y. Zhang, D. Zhou, Robust prescribed performance tracking control for free-floating space manipulators with kinematic and dynamic uncertainty, Aerosp. Sci. Technol. 71 (2017) 568–579.
[20] X. Yu, L. Chen, Modeling and observer-based augmented adaptive control of flexible-joint free-floating space manipulators, Acta Astronaut. 108 (2015) 146–155.
[21] Y. Jia, S. Xu, Decentralized adaptive sliding mode control of a space robot actuated by control moment gyroscopes, Chin. J. Aeronaut. 29 (3) (2016) 688–703.
[22] Y. Jia, A.K. Misra, Robust trajectory tracking control of a dual-arm space robot actuated by control moment gyroscopes, Acta Astronaut. 137 (2017) 287–301.
[23] E.T. Stoneking, Implementation of Kane's method for a spacecraft composed of multiple rigid bodies, in: AIAA Guidance, Navigation, and Control (GNC) Conference, Boston, MA, USA, Aug. 19–22, 2013, AIAA 2013-4649.
[24] J. Wei, D. Cao, L. Liu, W. Huang, Global mode method for dynamic modeling of a flexible-link flexible-joint manipulator with tip mass, Appl. Math. Model. 48 (2017) 787–805.
[25] X. Liu, H. Li, J. Wang, G. Cai, Dynamics analysis of flexible space robot with joint friction, Aerosp. Sci. Technol. 47 (2015) 164–176.
[26] W. Xu, J. Peng, B. Liang, Z. Mu, Hybrid modeling and analysis method for dynamic coupling of space robots, IEEE Trans. Aerosp. Electron. Syst. 52 (1) (2016) 85–98.
[27] W. Xu, Z. Hu, Y. Zhang, B. Liang, On-orbit identifying the inertia parameters of space robotic systems using simple equivalent dynamics, Acta Astronaut. 132 (2017) 131–142.
[28] S. Ulrich, J.Z. Sasiadek, Direct fuzzy adaptive control of a manipulator with elastic joints, in: AIAA Guidance, Navigation, and Control Conference, Minneapolis, MN, USA, Aug. 13–16, 2012, AIAA 2012-4620.
[29] S. Ulrich, J.Z. Sasiadek, I. Barkana, Modeling and direct adaptive control of a flexible-joint manipulator, J. Guid. Control Dyn. 35 (1) (2012) 25–39.
[30] S. Ulrich, J.Z. Sasiadek, I. Barkana, Nonlinear adaptive output feedback control of flexible-joint space robot manipulators, in: AIAA Guidance, Navigation, and Control (GNC) Conference, Boston, MA, USA, Aug. 19–22, 2013, AIAA 2013-4523.
[31] S. Ulrich, J.Z. Sasiadek, On the Simple Adaptive Control of Flexible-Joint Space Manipulators with Uncertainties, Aerospace Robotics II, Springer International Publishing, Switzerland, 2015, pp. 13–23.
[32] H.S. Jayakody, L. Shi, J. Katupitiya, N. Kinkaid, Robust adaptive coordination controller for a spacecraft equipped with a robotic manipulator, J. Guid. Control Dyn. 39 (12) (2016) 2699–2711.
[33] Y. Jia, Q. Hu, S. Xu, Dynamics and adaptive control of a dual-arm space robot with closed-loop constraints and uncertain inertial parameters, Acta Mech. Sin. 30 (1) (2014) 112–124.
[34] J. Virgili-Llop, J.V. Drew, R. Zappulla II, M. Romano, Laboratory experiments of resident space object capture by a spacecraft–manipulator system, Aerosp. Sci. Technol. 71 (2017) 530–545.
[35] W. Zhang, X. Ye, L. Jiang, Y. Zhu, X. Ji, X. Hu, Output feedback control for free-floating space robotic manipulators base on adaptive fuzzy neural network, Aerosp. Sci. Technol. 29 (2013) 135–143.
[36] P. Huang, F. Zhang, J. Cai, D. Wang, Z. Meng, J. Guo, Dexterous tethered space robot: design, measurement, control, and experiment, IEEE Trans. Aerosp. Electron. Syst. 53 (3) (2017) 1452–1468.